Surface expression of eastern Mediterranean slab dynamics: Neogene topographic and structural evolution of the southwest margin of the Central Anatolian Plateau, Turkey

Surface expression of eastern Mediterranean slab dynamics: Neogene topographic and structural evolution of the southwest margin of the Central Anatolian Plateau, Turkey

T. F. Schildgen,[1] D. Cosentino,[2,3] A. Caruso,[4] R. Buchwaldt,[5] C. Yıldırım,[1,6] S. A. Bowring,[5] B. Rojay,[7] H. Echtler,[1,6] and M. R. Strecker[1]

Received 13 September 2011; revised 18 January 2012; accepted 27 January 2012; published 16 March 2012.

[1] The southwest margin of the Central Anatolian Plateau has experienced multiple phases of topographic growth, including the formation of localized highs prior to the Late Miocene that were later affected by wholesale uplift of the plateau margin. Our new biostratigraphic data limit the age of uplifted marine sediments at the southwest plateau margin at 1.5 km elevation to <7.17 Ma, and regional lithostratigraphic correlations imply that the age is <6.7 Ma. Single-grain CA-TIMS U-Pb zircon analyses from a reworked ash within the marine sediments yield dates as young as 10.6 Ma, indicating a maximum age that is consistent with the biostratigraphy. Our structural measurements within the uplifted region and fault inversion modeling agree with previous findings in surrounding regions, with early contraction followed by strike-slip and extensional deformation during uplift. Focal mechanisms from shallow earthquakes show that the extensional phase has continued to the present. Broad similarities in the change in the tectonic stress regime (after 8 Ma) and the onset of surface uplift (after 7 Ma) imply that deep-seated process(es) caused post-7 Ma uplift. The geometry of lithospheric slabs beneath the plateau margin, Pliocene to recent alkaline volcanism, and the uplift pattern with accompanying normal faulting point toward slab tearing and localized heating at the base of the lithosphere as a probable mechanism for post-7 Ma uplift of the southwest margin. Considering previous work in the region, there appears to be an important link between slab dynamics and surface uplift throughout the Anatolian Plateau's southern margin.

Citation: Schildgen, T. F., D. Cosentino, A. Caruso, R. Buchwaldt, C. Yıldırım, S. A. Bowring, B. Rojay, H. Echtler, and M. R. Strecker (2012), Surface expression of eastern Mediterranean slab dynamics: Neogene topographic and structural evolution of the southwest margin of the Central Anatolian Plateau, Turkey, *Tectonics*, *31*, TC2005, doi:10.1029/2011TC003021.

1. Introduction

[2] The timing, magnitude, and mechanisms of surface uplift for major topographic features are critical for understanding long-term feedbacks among orogen growth, crustal deformation, and exhumation [e.g., *Willett*, 1999; *Hilley and Strecker*, 2004; *Stolar et al.*, 2007; *Roe et al.*, 2008; *Whipple*, 2009], changes in atmospheric circulation patterns [e.g., *Lenters and Cook*, 1997; *Seager et al.*, 2002], and the processes behind the development of features such as orogenic plateaus [e.g., *Allmendinger et al.*, 1997]. Knowing the uplift history can often help in differentiating among potential uplift mechanisms, as they are typically associated with specific spatial and temporal patterns of uplift [e.g., *Göğüş and Pysklywec*, 2008; *Duretz et al.*, 2011]. However, reconstructing surface uplift is challenging, with errors from most thermochronologic, cosmogenic, and stable isotope techniques typically ranging from 0.5 to 1 km [e.g., *Blisniuk and Stern*, 2005; *Quade et al.*, 2007; *Mulch and Chamberlain*, 2007; *Riihimaki and Libarkin*, 2007; *Sahagian and Proussevitch*, 2007]. Fortunately, different mechanisms leading to surface uplift are also often associated with specific tectonic stress regimes, deformation patterns, and magmatism, providing additional means to identify probable uplift mechanisms [e.g., *England and Houseman*, 1989; *Kay and Kay*, 1993; *Davies and von Blanckenburg*, 1995; *Schildgen et al.*, 2009]. The Central Anatolian Plateau, with a pristine record of uplifted marine sediments along its southern margin, multiple generations of faults recorded in carbonate rocks, and

[1]Institute of Earth and Environmental Science and DFG Leibniz Center for Surface Processes and Climate Studies, Universität Potsdam, Potsdam-Golm, Germany.
[2]Dipartimento di Scienze Geologiche, Università degli Studi Roma Tre, Rome, Italy.
[3]Istituto di Geologia Ambientale e Geoingeneria, CNR, Rome, Italy.
[4]Dipartimento di Scienze della Terra e del Mare, Università Palermo, Palermo, Italy.
[5]Department of Earth, Atmospheric and Planetary Sciences, Massachusetts Institute of Technology, Cambridge, Massachusetts, USA.
[6]Helmholtz-Zentrum Potsdam, Deutsches GeoForschungsZentrum, Potsdam, Germany.
[7]Jeoloji Mühendisliği Bölümü, Orta Doğu Teknik Üniversitesi, Ankara, Turkey.

0278-7407/12/2011TC003021

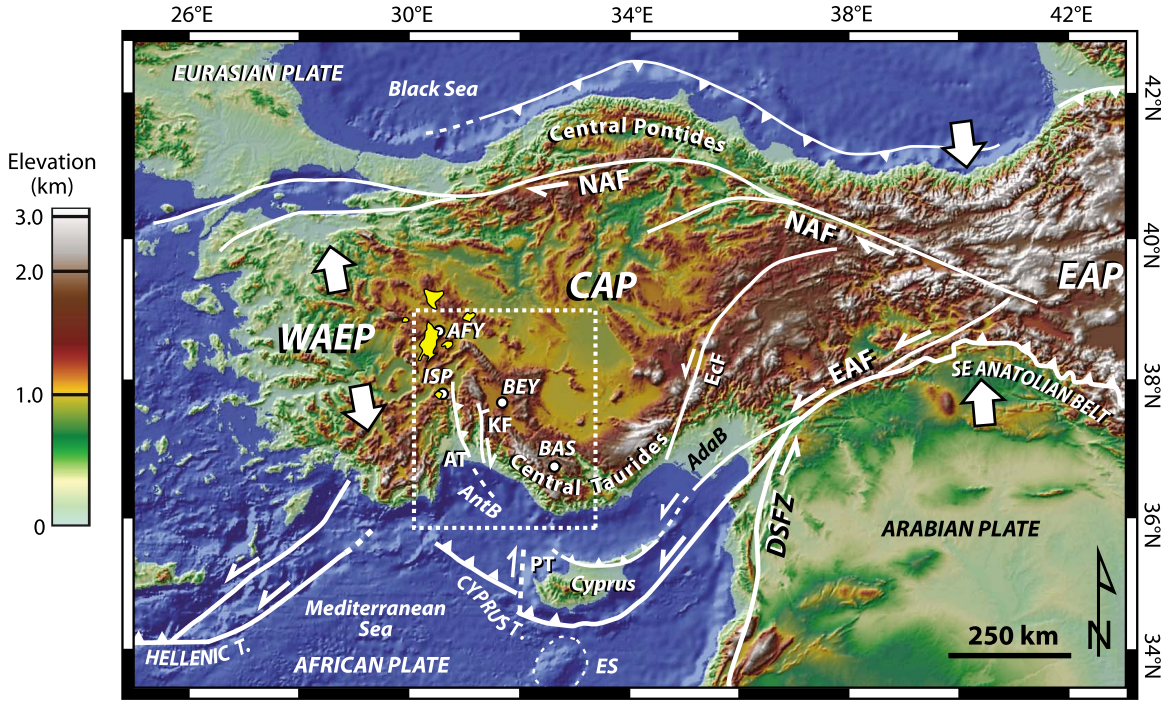

Figure 1. Tectonic setting of the Central Anatolian Plateau. WAEP, Western Anatolian extensional province; CAP, Central Anatolian Plateau; EAP, Eastern Anatolian Plateau; AT, Aksu Thrust; KF, Kirkkavak Fault; PT, Paphos Transform; EcF, Ecemiş Fault; NAF, North Anatolian Fault; EAF, East Anatolian Fault; DSFZ, Dead Sea Fault Zone; ISP, Isparta; BEY, Beyşehir; BAS, Başyayla; AFY, Afyon; AntB, Antalya Basin; AdaB, Adana Basin; ES, Eratosthenes Seamount. Yellow patches show outline of Miocene to Pliocene volcanic rocks with calc-alkaline to alkaline composition [from *Altunkaynak and Dilek*, 2006]. White lines indicate major tectonic plate boundaries and faults. Dotted white rectangle outlines region shown in Figure 2.

localized volcanism, provides all the key elements to discern the timing and magnitude of uplift, from which the associated uplift mechanisms can be inferred.

[3] The Central Anatolian Plateau marks the western end of the high topography associated with collision of the African and Arabian plates with Eurasia. Its location between the predominantly contractional Eastern Anatolian Plateau [e.g., *McKenzie*, 1970, 1978; *Şengör*, 1980; *Jackson and McKenzie*, 1984; *Jackson*, 1992; *McClusky et al.*, 2000; *Reilinger et al.*, 1997, 2006] and the predominantly extensional Western Anatolian province [e.g., *McKenzie*, 1970, 1978; *Le Pichon and Angelier*, 1979; *Jackson and McKenzie*, 1984; *McClusky et al.*, 2000; *Reilinger et al.*, 1997, 2006], together with its position northwest of the triple junction between the Arabian, Eurasian (Anatolian) and African plates, places it within a particularly complex tectonic setting (Figure 1). The Central Anatolian Plateau is separated from the Western Anatolian extensional province along the wedge-shaped, fault-bounded "Isparta Angle" [*Blumenthal*, 1963]. Fault kinematic measurements along the eastern margin of the Isparta Angle show Early to Middle Miocene contraction followed by strike-slip and normal faulting since the latest Miocene or Pliocene [*Glover and Robertson*, 1998]. The change in kinematics has been explained by two main hypotheses: processes originating in the upper mantle (lithospheric slabs and subduction), or processes related to regional plate motion and upper crustal deformation.

[4] From the upper mantle perspective, *Woodside* [1977] suggested that the changes signaled an end of "normal" subduction of the African plate beneath Anatolia within the last 5 Ma, with only limited underthrusting since that time. Along these lines, *Gans et al.* [2009] noted that slow Pn velocities east of Cyprus imply that slab break-off [e.g., *Davies and von Blanckenburg*, 1995] may have occurred in that region. *Cosentino et al.* [2012b] suggested the break-off could have induced post-Late Miocene surface uplift in that region, possibly in a manner analogous to that proposed for Eastern Anatolia [*Keskin*, 2003; *Şengör et al.*, 2003]. Farther west along the subduction zone beneath Central Anatolia, the slab tears interpreted from P wave tomography data [*Biryol et al.*, 2011] could result in localized asthenospheric upwelling. Models of such upper mantle processes predict surface uplift patterns that are characterized by wavelengths of 100 km or more and accompanying upper crustal extension [*Davies and von Blanckenburg*, 1995; *Duretz et al.*, 2011; *Göğüş and Pysklywec*, 2008].

[5] From the tectonic plate perspective, *Glover and Robertson* [1998] expanded on ideas originally presented by *Rotstein* [1984] and *Taymaz et al.* [1991] in suggesting that the kinematic changes near the Isparta Angle were related to changes in plate motion. In this scenario, the initially westward-extruding Anatolian plate was inferred to have broken into two counter-clockwise (CCW) rotating domains

(Western and Central Anatolia). Since that time, paleomagnetic data show that most of the CCW rotation of Central Anatolia has occurred since Pliocene time [*Piper et al.*, 2010]. Block models fit to geodetic velocity data [*Reilinger et al.*, 2006] also require Central Anatolia to undergo CCW rotation. Surface uplift related to such horizontal plate motions would be restricted to areas where faults are in restraining orientations with respect to plate movement, and should be accompanied by upper crustal shortening. This latter model of surface uplift has been suggested for the northern margin of the Central Anatolian Plateau, where the North Anatolian fault forms a broad restraining bend and the Central Pontides are characterized by active shortening [*Yıldırım et al.*, 2011]. If Central Anatolia has indeed been undergoing CCW rotation, the southern margin of the plateau may also be a regionally important compressional zone, in contrast with the tensional stress regime and extensional tectonics expected from uplift above a slab tear or break-off.

[6] In light of these studies, surface uplift along the southwest margin of the Central Anatolian Plateau (western Central Taurides, bordering the Isparta Angle to the east) could relate to processes associated with lithospheric slab dynamics and/or regional tectonic motions. Here we integrate new data on the timing, magnitude, and pattern of surface uplift of the southwest margin of the Central Anatolian Plateau with analyses of changes in the regional tectonic stress regime to test these two alternatives. Our timing constraints on surface uplift are derived from biostratigraphy of uplifted marine sediments and from radiometric dating of an intercalated volcanic ash. To integrate our chronologic data from the southwest plateau margin with regional deformation patterns, we reconstruct the cumulative post-Late Miocene surface uplift pattern throughout the region based on geomorphic and stratigraphic reference surfaces. Finally, we combine the data on surface uplift timing and patterns with fault plane measurements from the southwest plateau margin and fault inversion modeling to assess temporal changes in crustal stress regimes. Specifically, we focus on changes that are broadly coeval with the start of surface uplift to assess whether horizontal plate motions or lithospheric slab dynamics are most likely to have contributed to plateau margin uplift.

2. Geologic and Tectonic Setting

[7] The Anatolian microplate, which separates the Eurasian plate to the north from the African and Arabian plates to the south, is bounded by the dextral North Anatolian fault to the north, the sinistral East Anatolian fault to the southeast, and the Aegean (Hellenic)-Cyprus subduction zone to the south and west. The Tauride Mountains form the high topography along the southern margin of the Anatolian microplate, with the Isparta Angle separating the Western Taurides and the South Aegean (Hellenic) Arc from the Central Taurides and the Cyprus Arc (Figure 1). *Barka and Reilinger* [1997] used differences in GPS velocities and greater extension above the Aegean slab compared to above the Cyprus slab to argue that a tear may exist between the two. Volcanism between the Kırka-Afyon and Isparta regions (Figure 1) shows a progression from Early Miocene (K/Ar ages of 21–17 Ma [*Basang et al.*, 1977; *Yalçın*, 1990]) calc-alkaline rocks in the north to Pliocene (4.7 ± 0.5 and 4.1 ± 0.2 Ma [*Lefèvre et al.*, 1983]) alkaline rocks in the south [*Yağmurlu et al.*, 1997; *Alıcı et al.*, 1998; *Francalanci et al.*, 2000]. The change to alkaline chemistry has been linked to the onset of extension [*Yağmurlu et al.*, 1997; *Alıcı et al.*, 1998; *Francalanci et al.*, 2000] and potentially upwelling asthenosphere through a break or tear in the subducting slab [*Francalanci et al.*, 2000; *Dilek and Altunkaynak*, 2009; *Dilek and Sandvol*, 2009]. In contrast, calc-alkaline compositions characterize the whole suite of Late Miocene to Pliocene rocks between Beyşehir and the Konya Basin, which has been inferred to result from subduction of the Cyprus slab [*Temel et al.*, 1998]. Analyses of gravity data and seismicity similarly suggest that a slab is actively subducting between the Isparta Angle and western Cyprus [*Kalyoncuoğlu et al.*, 2011]. Recent P wave tomography interpretations largely support these geodynamic interpretations, including a large tear between the Cyprus and Aegean slabs, a minor tear between western Cyprus and the Isparta Angle (approximately along the Paphos transform (PT), Figure 1), and apparently no slab to the east of Cyprus [*Biryol et al.*, 2011]. Some authors have suggested that Cyprus itself overlies a locked portion of the subduction zone [e.g., *Harrison et al.*, 2008]. Such locking may be linked to the collision of the Erathosthenes Seamount with the Cyprus Arc, as the collision appears to have induced structural changes throughout the E Mediterranean [*Schattner*, 2010].

[8] Individual morpho-tectonic domains within the region show some similarities in their deformation histories. *Glover and Robertson* [1998] showed that within the Isparta Angle's Köprü Basin (Figure 2), early contractional deformation was followed by dextral strike-slip and normal faulting. The contractional phase could be related to either tightening due to inward rotation of the Isparta Angle limbs starting in Eocene time [e.g., *Frizon de Lamotte et al.*, 1995; *Kissel and Poisson*, 1986; *Kissel et al.*, 1993; *Morris and Robertson*, 1993; *van Hinsbergen et al.*, 2010] or westward extrusion of the Anatolian microplate [*McKenzie*, 1978; *Şengör and Yılmaz*, 1981] starting in Middle Miocene time [*Şengör et al.*, 2005]. *Monod et al.* [2006] similarly suggested that normal faulting played a major role in the latest phase of landscape development in the high-relief region of the western Central Taurides. These interpretations contrast with those of *Deynoux et al.* [2005], who inferred the most recent deformation to be contractional; however, that interpretation relied on folding of Early to Middle Miocene (and not necessarily younger) units. *Deynoux et al.* [2005] also described an E-W striking normal fault that they suggested is one of the youngest structures within the Köprü Basin. Analogous changes have been reported to the NE in the Akşehir graben (Figure 2), where *Koçyiğit et al.* [2000] described early reverse faulting that preceded normal faulting, the latter of which induced growth strata in Upper Miocene, Pliocene, and younger sediments. Also, in the plateau realm along the western margin of the Tuz Gölü basin, normal and strike-slip (or transfer) faulting followed contractional deformation [*Özsayın and Dirik*, 2011].

[9] In contrast with these areas within or immediately adjacent to the plateau, regions to the south and west are characterized by sustained contractional deformation. For example, offshore seismic reflection data from the Antalya Basin reveal contractional deformation from Middle to Late Miocene time [*Işler et al.*, 2005]. A major change occurred

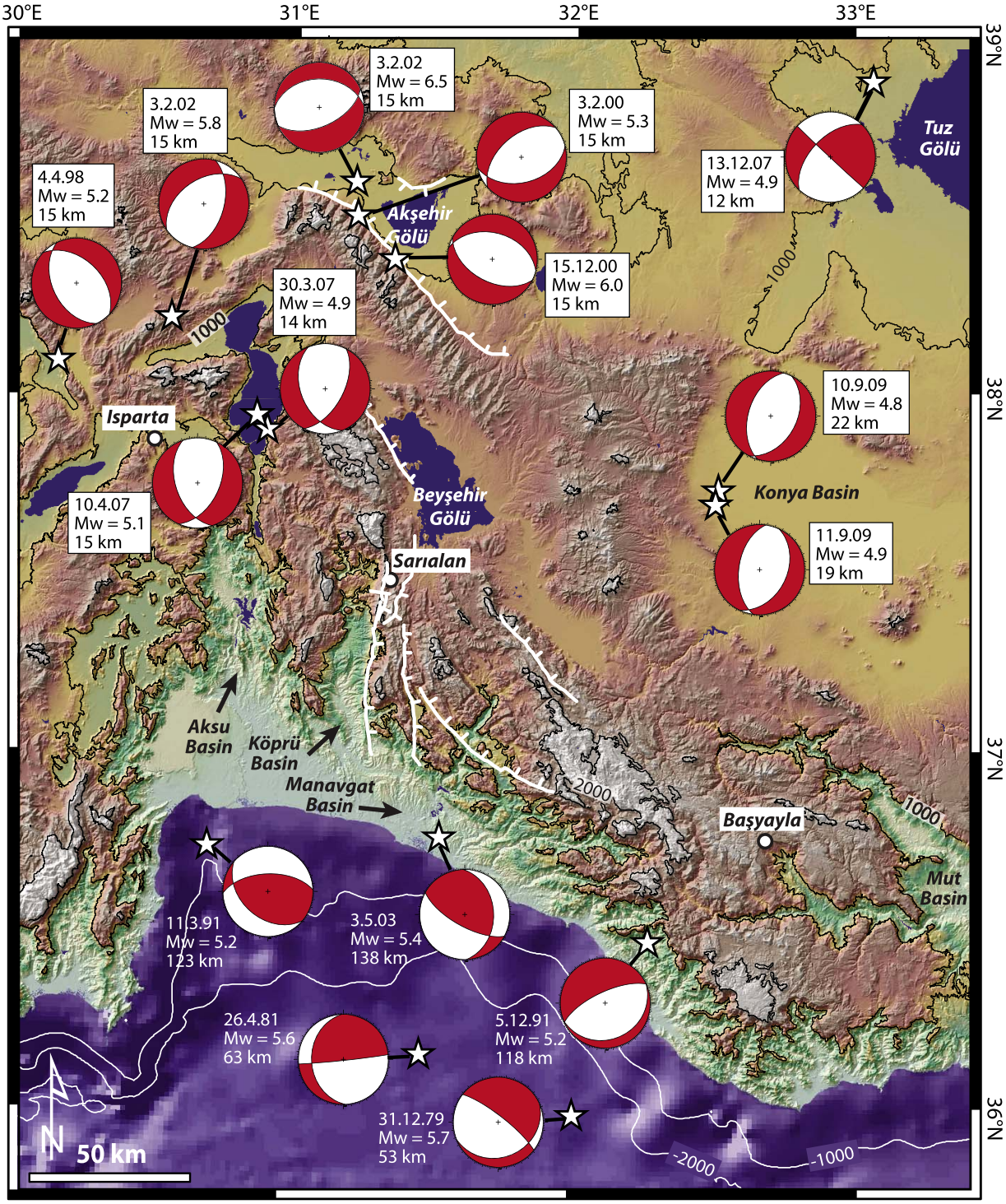

Figure 2. Earthquake focal mechanisms in the vicinity of the study region. Labels for focal mechanisms indicate date, magnitude, and hypocenter depth. Contour lines on topography and bathymetry in 1000-m intervals. Late Miocene or younger faults shown in white, with dashes indicating normal movement.

at the Miocene/Pliocene transition, with emergence of the Manavgat and Aksu basins (Figure 2) and strain partitioning into two domains that extend eastward toward the Adana Basin: extension/transtension close to shore, and a contractional zone to the south that aligns with thrusts in the Aksu Basin and in northern Cyprus [*Işler et al.*, 2005; *Aksu et al.*, 2005]. This interpretation is consistent with Pliocene and younger thrusting in the Aksu valley [*Robertson et al.*, 2003; *Poisson et al.*, 2003, 2011].

[10] Today, earthquake focal mechanisms in the region reveal tensional stresses for upper crustal (14–21 km depth) hypocenters in the western Central Taurides and transtensional stresses near Tuz Gölü (Figure 2). Compressional focal mechanisms are only found south of the study area at

63 to 138 km depth, which are most likely associated with subduction of the Cyprus slab [e.g., *Kalyoncuoğlu et al.*, 2011]. The two deep (118 and 53 km depth) focal mechanisms revealing tension between 32° and 32.5°E lie above what is interpreted as a minor tear in the slab subducting beneath that region based on P wave tomography data [*Biryol et al.*, 2011].

3. Geomorphic and Stratigraphic Evidence for Surface Uplift

[11] Surface uplift along the southwest plateau margin is recorded in both the landscape morphology and within the stratigraphic record. The western Central Taurides are marked by a series of horsts capped by relatively low-relief paleosurfaces. *Monod et al.* [2006] observed that the paleosurfaces are incised by dry, beheaded, NE-SW-oriented paleovalleys. These paleovalleys abruptly terminate at precipitous slope breaks above the modern drainage system (similar to hanging valleys in formerly glaciated terrain, although no evidence of glaciation was observed by *Monod et al.* [2006]), and frequently have hanging paleo-tributary valleys. *Monod et al.* [2006] used the landscape morphology and provenance analysis of tracer pebbles to argue that the paleovalleys were part of a continuous, southwest-flowing drainage network that was affected by two phases of surface uplift and/or base level fall. The first phase stranded smaller tributaries above the main paleovalleys, and the second phase disrupted the main valley network. Tortonian marine sediments preserved close to the floor of the modern drainage system record a final transgression that affected the region prior to regional surface uplift [*Deynoux et al.*, 2005]. The timing of the paleovalley network disruption, together with the age of the uplifted marine sediments, limits the timing and magnitude of surface uplift in the region.

3.1. Age of the Paleovalley Network

[12] Given the close link between surface uplift and paleovalley network abandonment, the timing of paleovalley-derived conglomerate deposition can offer one perspective on the timing of surface uplift. *Monod et al.* [2006] suggested that the paleovalley network drained to the Manavgat Basin (Figure 2), given the presence of tracer pebbles at the northern margin of the basin. In the Manavgat Basin, Burdigalian to early Langhian terrestrial to marine conglomerates of the Tepekli Formation were deposited with south to southwest paleoflow directions [*Akay and Uysal*, 1985; *Flecker et al.*, 1998; *Karabıyıkoğlu et al.*, 2000], followed by early Tortonian to Messinian south- to southwest-directed marine fan-delta conglomerates interlayered with mudstones, debris flows, and turbidites of the Karpuzçay Formation [e.g., *Bizon et al.*, 1974; *Akay et al.*, 1985; *Akay and Uysal*, 1985; *Karabıyıkoğlu et al.*, 2000]. *Flecker et al.* [1995] and *Karabıyıkoğlu et al.* [2000] interpreted the change in facies within the Karpuzçay Formation, together with minimal deformation of the basin, to indicate syndepositional uplift of the hinterland to the N and NE.

[13] Conglomerate deposition shifted to the modern offshore realm of the Antalya Basin during the late Messinian. Offshore seismic data shows a package of conglomerates (Unit 1 of *Işler et al.* [2005]) that have been correlated with the conglomerates of the Handere Formation in the Adana Basin (Figure 1) based on similarity in facies and their position above the regional M reflector. Although the conglomerates of the Handere Formation have been traditionally interpreted to be Pliocene in age [e.g., *Schmidt*, 1961; *Yalçın and Görür*, 1984; *Gürbüz and Kelling*, 1993; *Nazik*, 2004; *Burton-Ferguson et al.*, 2005; *Darbaş and Nazik*, 2010], the recent identification of late-Lago-Mare biofacies (*Loxocorniculina djafarovi* Zone) within interlayered marls of the Handere Formation in the Adana Basin [*Cosentino et al.*, 2010] demonstrates a latest Messinian age (5.45 to 5.33 Ma). Importantly, *Jaffey and Robertson* [2005] also described sedimentary evidence for margin uplift along basins flanking the SE plateau margin to the north, where coarse conglomerates of Pliocene and younger age rest on an angular unconformity. Although correlations between the conglomerates of the Antalya and Adana basins are currently tentative, the sedimentary record provides one important line of evidence that surface uplift of the southern plateau margin had started by late Messinian time.

3.2. Uplifted Marine Sediments

[14] Patches of marine sediments along the uplifted southwest plateau margin provide maximum age limits on the start of the most recent surface uplift. From marine marls near the village of Sarıalan (ca. 1400 m a.s.l., Figure 2), *Deynoux et al.* [2005] identified nannofossil biozone NN9-NN10 (10.3 to 8.3 Ma). *Flecker et al.* [2005] also reported a "late Tortonian (Messinian)" age, although the described planktonic foraminifera assemblage is associated with the late Tortonian.

[15] The Late Miocene age estimates of 1.4-km-high marine sediments along the southwest plateau margin are broadly similar to the ages of 2-km-high marine sediments capping the central portion of the southern plateau margin in the Central Taurides. Near the town of Başyayla (Figure 2), *Cosentino et al.* [2012b] limited the age of the stratigraphically highest marls to 8.35 to 8.10 Ma (late Tortonian) using biostratigraphy and magnetostratigraphy. Given that the age of uplifted marine sediments provides a maximum age limit for the start of surface uplift, regional observations imply that the southern plateau margin started to be uplifted after late Tortonian time (8 Ma) based on uplifted marine sediments near Başyayla and Sarıalan, and before late Messinian time (5.45 Ma) based on the sedimentary record of the Adana Basin and possibly also the Antalya Basin.

4. New Constraints on Surface Uplift Timing

[16] We define new ages of marine sediments near Sarıalan based on planktonic and benthic foraminifera from a composite section that includes ca. 100 m of marine sediments above the previously described section [*Deynoux et al.*, 2005]. Regional correlations with other sections from Cyprus, Crete, and Sicily allow us to better constrain the age of the uppermost part of the marine sediments in the Sarıalan area, which shows an abrupt change in lithology similar to other Mediterranean sections. Age constraints on these stratigraphically higher sediments help to further limit the temporal gap between the previous maximum and minimum age estimates for the onset of surface uplift along the southern plateau margin. Because the marine sediments were deposited close to sea level, their current elevation also illustrates

the cumulative surface uplift and associated long-term average uplift rate of the southwest plateau margin. Single-crystal zircon U-Pb ages from a reworked ash near the base of the section provide an independent test of the biostratigraphic age.

4.1. Sampled Marine Section

[17] All samples were collected from exposed sections close to the village of Sarıalan (Figure 2), between the locations N37° 30.840′ E 31° 21.707′ (1431 m elevation) and N37° 30.091′ E 31° 21.214′ (1535 m elevation). The section (Figure 3) starts with patch reefs interlayered with marls, silty marls, and a 5-cm-thick reworked ash layer. The patch reefs and marls transition upward to coarse sandstones rich in large benthic foraminifera (*Heterostegina* spp.), which become finer-grained upsection and are eventually replaced by biocalcarenites rich in *Heterostegina* spp. and other benthic foraminifera within a micritic carbonate matrix. Higher in elevation are grayish silty marls rich in planktonic foraminifera, which transition upward to a cyclic alternation of silty marls with cm-scale carbonate horizons. These cyclic alternations pass upwards into thinly laminated brownish marls and clays rich in biosiliceous remains (mainly sponge spicules) and organic matter.

[18] The Sarıalan section is reported to overlie Mesozoic basement rocks across a normal fault contact [*Monod et al.*, 2006]. Although we found no clear exposure of the contact, most of the exposed section is sub-horizontal or slightly tilted (up to 12°) with local, minor (centimeter to decimeter) high-angle fault offsets. At the base of the section, pebbles with *Lithofaga* borings attest to a nearshore environment. Benthic foraminifera, which occur throughout the section, record changes in paleodepth from littoral inner shelf (ca. 10 m depth) to circalittoral (>80–100 m depth) environments. The highest sediments in the section, characterized by thinly laminated brownish marls with abundant shallow-water benthic fauna (>10 m depth) and biosiliceous remains, are overlain by landslide blocks derived from the ridge-forming Mesozoic carbonates to the west. These blocks may cover stratigraphically higher marine sediments, but likely have helped to preserve this small patch of easily erodible material.

4.2. Sample Preparation and Analysis

4.2.1. Biostratigraphic Samples

[19] We prepared 13 hard/oyster samples for thin section analyses, and 16 "soft" samples from the marls and silty marls horizons for benthic and planktonic foraminifera content. For foraminifera analyses, ca. 200 g of sample were soaked and diluted in water to disaggregate the sediments without damaging the specimens, then washed under running water through 250 μm, 125 μm and 63 μm mesh sieves. A semiquantitative analysis was performed in all samples in order to identify foraminiferal species and to assess their diversity and abundance.

4.2.2. High Precision CA-TIMS Geochronology

[20] We dried and sieved a ca. 3 kg of material including the reworked ash from the basal part of the Sarıalan section (sample SAR-B-1), and processed the <500 μm fraction using standard water table, magnetic, and heavy liquid separation techniques. Zircon grains were hand-selected for analysis from the least magnetic fraction based on the absence of cracks, inclusions, and surface contamination.

[21] To minimize the effects of Pb loss, the grains were subjected to a version of the thermal annealing and acid leaching (also known as chemical abrasion or CA-TIMS) technique of *Mattinson* [2005] prior to isotope dilution thermal ionization mass-spectrometry (ID-TIMS) analyses using a mixed ^{205}Pb-^{233}U-^{235}U tracer solution (spike). Details of zircon pre-treatment, dissolution and U and Pb chemical extraction procedures are described by *Ramezani et al.* [2007].

[22] U and Pb isotopic measurements were performed on a VG Sector-54 multicollector thermal ionization mass spectrometer at MIT. Pb and U were loaded together on a single Re filament in a silica-gel/phosphoric acid mixture [*Gerstenberger and Haase*, 1997]. Pb isotopes were measured by peak-hopping using a single Daly photomultiplier detector and U isotopic measurements were made in static mode using multiple Faraday collectors. Details of fractionation and blank corrections are given in Table 1. Data reduction, age calculation, and the generation of concordia plots were carried out using the method of *McLean et al.* [2011], and the statistical reduction and plotting program REDUX [*Bowring et al.*, 2011]. Unless otherwise noted, U-Pb errors on analyses from this study are reported as: ±X/Y/Z, where X is the internal error in absence of all systematic errors, Y includes the tracer calibration error, and Z includes both tracer calibration and decay constant errors of *Jaffey et al.* [1971].

4.3. Biostratigraphic, Lithostratigraphic and Geochronologic Results

4.3.1. Biostratigraphic Age Limits

[23] We identified benthic and planktonic foraminifera assemblages in all of the analyzed "soft" samples of the Sarıalan section. At the base of the Sarıalan section within the marls and coral patch-reefs (SAR 20 and SAR-B 0 samples), we identified *Globigerinoides extremus*, whose First Occurrence (FO) is at 8.35 Ma [*Sprovieri et al.*, 1996]. Moreover, the occurrence of very rare *Sphaeroidinellopsis* spp. in SAR-B 0, whose First Regular Occurrence (FRO) has been calibrated in several Mediterranean sections at ca. 7.9 Ma [*Krijgsman et al.*, 1995; *Kouwenhoven et al.*, 1999; *Hüsing et al.*, 2009], further limits the age of the marls within the coral patch-reefs as younger than the FRO of *Sphaeroidinellopsis* spp.

[24] Upsection, above the *Heterostegina*-bearing layers, the Sarıalan section records the deepest marine environment (SAR-C 1 sample: >80–100 m depth) with rich planktonic foraminifera assemblages characterized by abundant *Sphaeroidinellopsis* spp., common *Orbulina universa*, rare *Globorotalia menardi* sx coiling, and other planktonic foraminifera. Starting with sample SAR-C 2, *Sphaeroidinellopsis* spp. becomes very rare. Sample SAR-C 1 likely represents the acme of *Sphaeroidinellopsis* spp., which could be placed at ca. 7.8 Ma, between its FRO (7.92 Ma [*Hüsing et al.*, 2009]) and LRO (7.72 Ma [*Hüsing et al.*, 2009]).

[25] The uppermost part of the Sarıalan section, at the start of the SAR-A samples, records the disappearance of most of the benthic foraminifera that occur in the older samples. Among others, the oxyphilic species *Siphonina reticulata*, which was found throughout the section starting from the basal sample (SAR 20), disappears starting from sample SAR-A 0. *Siphonina reticulata* disappeared from deep marine

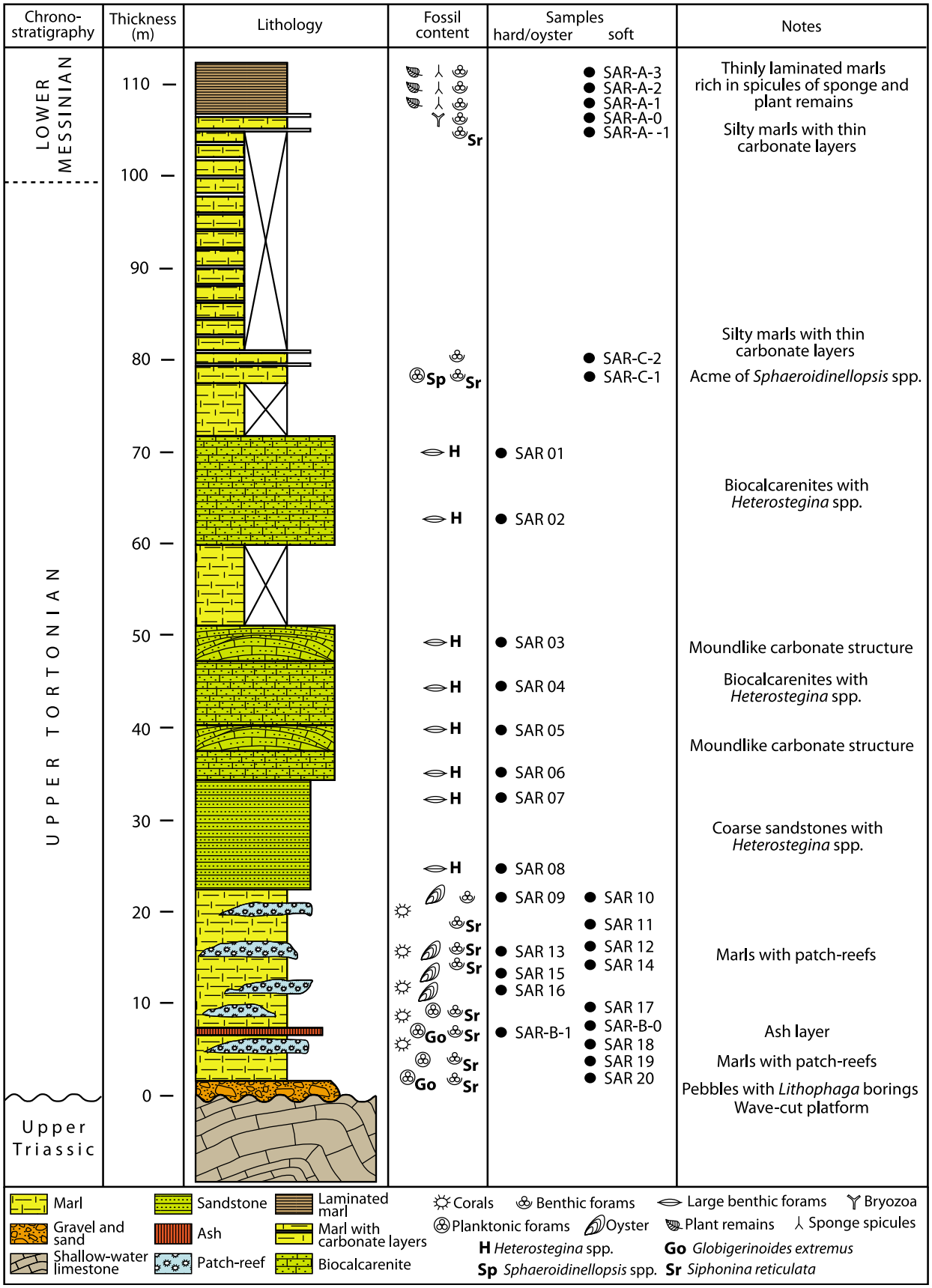

Figure 3. Stratigraphic log of Sarıalan section. "Soft" samples are marls collected for foraminifera analysis, while "hard/oyster" samples were collected for thin section analysis.

Table 1. U-Pb Isotopic Data and Dates of Individual Zircon Grains From Reworked Ash Sample SAR-B-1[a]

	Composition				Isotopic Ratios							Dates (Ma)				
Grain	Th/U[b]	Pb*[c] (pg)	Pbc[d] (pg)	Pb*/Pbc[e]	$^{206}Pb/^{204}Pb$[f]	$^{206}Pb/^{238}U$[g,h]	±2σ (%)	$^{207}Pb/^{235}U$[g]	±2σ (%)	$^{207}Pb/^{206}Pb$[g,h]	±2σ (%)	$^{206}Pb/^{238}U$[h,i]	±2σ (abs.)	$^{207}Pb/^{235}U$[i]	±2σ (abs.)	$^{207}Pb/^{206}Pb$[h,i]	±2σ (abs.)	Correlation Coefficient
z1	0.69	0.4	0.41	0.94	71.6	0.00166	1.037	0.012	14.42	0.050934	13.642	10.71	0.11	11.79	1.7	237.8	314.6	0.78
z3	0.37	0.7	0.45	1.55	114.1	0.00166	0.669	0.010	10.21	0.045643	9.653	10.67	0.07	10.53	1.1	−21.2	233.6	0.85
z4	0.32	1.7	0.50	3.39	227.0	0.00531	0.303	0.051	2.68	0.069056	2.458	34.15	0.10	50.09	1.3	900.4	50.7	0.75
z6	0.69	9.1	4.92	1.85	122.8	0.01598	0.576	0.127	6.03	0.057697	5.606	102.18	0.58	121.49	6.9	518.3	123.1	0.75
z7	0.50	0.8	0.49	1.67	118.3	0.00166	0.599	0.010	10.49	0.045317	10.011	10.66	0.06	10.45	1.1	−38.6	243.1	0.82
z8	0.69	1.5	0.63	2.43	156.5	0.00165	0.401	0.011	5.71	0.047047	5.407	10.65	0.04	10.83	0.6	51.6	129.1	0.80
z9	3.55	6.8	0.52	13.12	451.3	0.00166	0.504	0.011	1.68	0.047598	1.647	10.68	0.05	10.99	0.2	79.3	39.1	0.61
z10	0.80	0.9	0.54	1.71	112.8	0.00164	0.599	0.011	8.78	0.046316	8.325	10.60	0.06	10.61	0.9	14.1	200.1	0.78

[a]Blank composition: $^{206}Pb/^{204}Pb = 18.24 \pm 0.21$; $^{207}Pb/^{204}Pb = 15.34 \pm 0.16$; $^{208}Pb/^{204}Pb = 37.35 \pm 0.20$
[b]Th contents calculated from radiogenic ^{208}Pb and the $^{207}Pb/^{206}Pb$ date of the sample, assuming concordance between U-Th and Pb systems.
[c]Total mass of radiogenic Pb.
[d]Total mass of common Pb.
[e]Ratio of radiogenic Pb (including ^{208}Pb) to common Pb.
[f]Measured ratio corrected for fractionation and spike contribution only.
[g]Measured ratios corrected for fractionation, tracer, blank and initial common Pb.
[h]Corrected for Initial Th/U disequilibrium using radiogenic ^{208}Pb and Th/U [magma] = 2.8.
[i]Isotopic dates calculated using the decay constants $\lambda_{238} = 1.55125E\text{-}10$ and $\lambda_{235} = 9.8485E\text{-}10$ [*Jaffey et al.*, 1971].

environments of the Mediterranean around 7.17 Ma [*Kouwenhoven et al.*, 1999, 2003, 2006] and did not return until the base of the Zanclean (5.33 Ma, Early Pliocene) [*Sgarrella et al.*, 1999; *Di Stefano et al.*, 1999].

[26] The planktonic/benthic (P/B) ratio and the benthic assemblages from the upper part of the Sarıalan section (where *S. reticulata* disappears) indicate an inner shelf littoral environment (>30 m deep). Compared to the Tochni section (Figure 4), the disappearance of *S. reticulata* happens closer to the first occurrence of micro-scale laminites in the Sarıalan section. Although we are not able to independently date the layer where *S. reticulata* disappears in the Sarıalan section, the synchronicity of the abrupt lithologic change recognized in all the Late Miocene eastern Mediterranean sections ("y" event in Figure 4, see section 4.3.2) suggests a delay in the disappearance of *S. reticulata* in shallow-water environments. Thus, in the Sarıalan section, this bioevent should be younger than 7.17 Ma. The last three samples of the Sarıalan section (SAR-A 1–3) record a major decrease of foraminiferal diversity. In particular, planktonic foraminifera are very rare while benthic species typical of shallow water (for instance *Elphidium* spp. and *Lobatula lobatula*) become dominant. In these last three samples, which are rich in organic matter, gastropods and biosiliceous remains as sponge spicules are very common.

4.3.2. Lithostratigraphic Age Limits

[27] The lithostratigraphy of the Sarıalan section shows similarities with other Mediterranean Late Miocene sedimentary sections, especially in its distinct lithologic change in the uppermost part of the section. Abrupt changes in lithology from carbonates to diatomites/sapropels and then to evaporites are recorded in upper Tortonian-Messinian successions throughout the Mediterranean, including sections in Spain [*Pérez-Folgado et al.*, 2003] Crete [*Santarelli et al.*, 1998; *Faranda et al.*, 2008], Cyprus [*Krijgsman et al.*, 2002; *Kouwenhoven et al.*, 2006; *Orszag-Sperber et al.*, 2009], Sicily [*Krijgsman et al.*, 1995; *Bellanca et al.*, 2001; *Rouchy and Caruso*, 2006], the central Apennines [*Sampalmieri et al.*, 2010], and the northern Apennines [*Roveri et al.*, 2003; *Roveri and Manzi*, 2006]. These basin-wide lithologic changes are mainly due to discrete steps of restriction of the connection between the Mediterranean Basin and the Atlantic Ocean [*Kouwenhoven et al.*, 2006] and related changes in basin-wide circulation patterns.

[28] Before the Messinian Salinity Crisis (MSC), the Mediterranean experienced at least two basin-wide restriction events. These events are recorded at 7.17 Ma by changes in benthic foraminifera assemblages [e.g., disappearance of *Siphonina reticulata* and other oxyphilic species, *Kouwenhoven et al.*, 1999, 2003, 2006] and at 6.7–6.8 Ma by the abrupt shift in lithofacies patterns from carbonate to sapropelitic/diatomitic deposition [*Santarelli et al.*, 1998; *Bellanca et al.*, 2001; *Krijgsman et al.*, 2002; *Pérez-Folgado et al.*, 2003, *Kouwenhoven et al.*, 2006; *Orszag-Sperber et al.*, 2009]. The latter event was recognized in sections throughout the eastern Mediterranean, including Metochia (Gavdos [*Krijgsman et al.*, 1995; *Santarelli et al.*, 1998]), Faneromeni (Crete [*Krijgsman et al.*, 1995; *Santarelli et al.*, 1998]), Messarà Basin (Crete [*Faranda et al.*, 2008]), Panasos (Crete (D. Cosentino and T. F. Schildgen, unpublished data, 2010)), Pissouri (Cyprus [*Krijgsman et al.*, 2002; *Kouwenhoven et al.*, 2006]), and Tochni (Cyprus

[*Orszag-Sperber et al.*, 2009). According to *Krijgsman et al.* [2002], although the astronomical tuning for the Pissouri section between 7.0 and 6.5 Ma is not fully resolved, the transition to sapropelitic sediments in the Pissouri Motorway Section happens one precessional cycle later than the Last Occurrence (LO) of *Globorotalia nicolae*, which in other Mediterranean sections was astronomically dated at 6.722 Ma [*Hilgen et al.*, 1995]. In the same section, just two precessional cycles above the *G. nicolae* LO, the sediment starts to show micro-scale laminite facies [*Kouwenhoven et al.*, 2006]. Four precessional cycles later the sediments become rich in biosiliceous remains (mainly sponge spicules) [*Krijgsman et al.*, 2002; *Kouwenhoven et al.*, 2006].

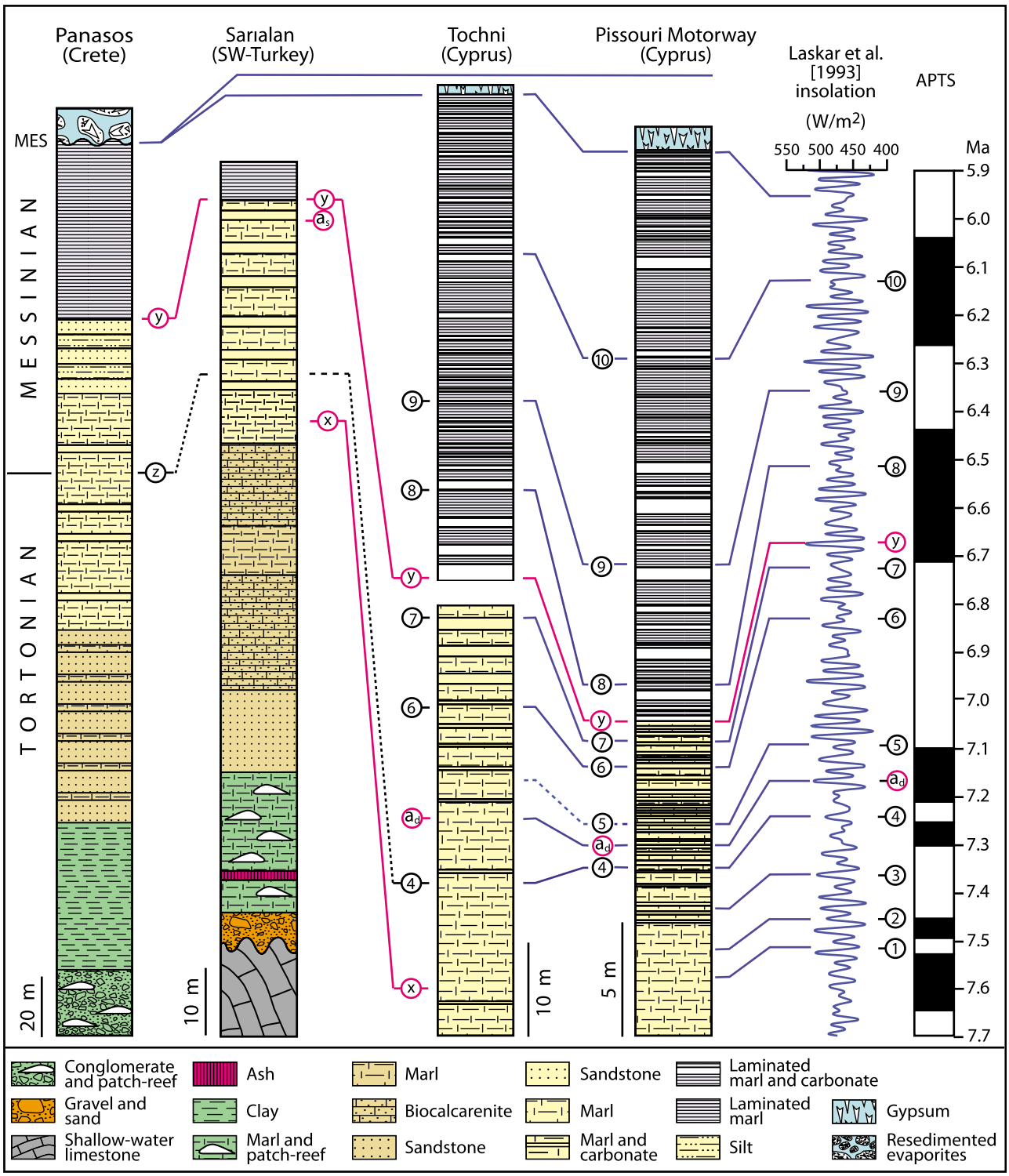

Figure 4

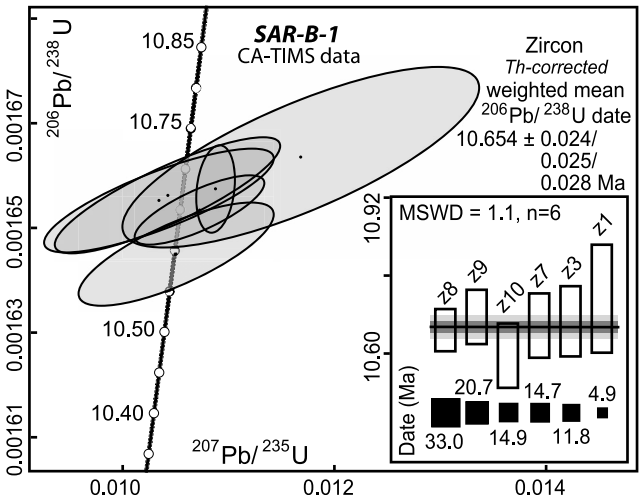

Figure 5. Concordia plot with 2σ error ellipses of the six CA-TIMS U-Pb single-grain zircon analyses used to calculate a date for sample SAR-B-1 from the reworked ash. In inset plot, all sample analyses are shown, with white boxes showing the statistically concordant results and black boxes showing disconcordant (and older) results. The error in the U-Pb date is shown as ±X/Y/Z, where X is the internal error in absence of all systematic errors, Y includes the tracer calibration error, and Z includes both tracer calibration and decay constant errors of *Jaffey et al.* [1971].

[29] In the Tochni section, *Orszag-Sperber et al.* [2009] found the same bioevents and lithological changes that were previously proposed for the Pissouri section [*Krijgsman et al.*, 2002; *Kouwenhoven et al.*, 2006]. In particular, using the calibration of the Pissouri bioevents [*Krijgsman et al.*, 2002], they found the disappearance of *S. reticulata* at 7.17 Ma, the reduction of benthic foraminifera at around 6.8 Ma, and the increase of detrital grains at 6.5 Ma, together with a drastic reduction of biodiversity in the fossil assemblages. Moreover, in the upper part of the Tochni section, *Orszag-Sperber et al.* [2009] found sponge remains.

[30] In the Sarıalan section, the thinly laminated brownish marls rich in biosiliceous remains (sponge spicules) occurring above the disappearance of *S. reticulata* could correlate the sponge-spicule-bearing, micro-scale laminite facies of the Pissouri Motorway Section in Cyprus. Although in the Pissouri section this lithological change happened within the unresolved astronomical tuning interval (7.0–6.5 Ma [*Krijgsman et al.*, 2002]), it could be reasonably placed at ca. 6.7 Ma, as in other Upper Miocene Mediterranean sections [*Krijgsman et al.*, 2002; *Kouwenhoven et al.*, 2006].

4.3.3. U-Pb Zircon Ages From Reworked Ash

[31] Small (150–200 μm), clear, euheadral zircons with sharp edges dominate the zircon population of sample SAR-B-1. Nine grains without inclusions were selected for analysis. Six of the nine grains are statistically concordant with a slight variation in the $^{206}Pb/^{238}U$ dates and yielding a $^{206}Pb/^{238}U$ weighted mean date of 10.654 ± 0.024/0.025/0.028 Ma (MSWD = 1.1) (Figure 5). The remaining three grains are discordant and significantly older. These grains have been interpreted as containing an inherited component and were therefore excluded from the date calculation.

5. Paleotopographic Reconstruction

[32] We used marine sediments capping the southern margin of the Central Anatolian Plateau as a reference surface to reconstruct the pattern of cumulative plateau margin deformation since the Late Miocene. To do this, we first manually selected points within mapped Upper Miocene neritic marine sediments from 1:500,000 scale MTA maps [*Şenel*, 2002; *Ulu*, 2002] and along onlap surfaces and paleoshoreline indicators from field and Google Earth observations (Figure 6a). We defined their elevations with Shuttle Radar Topography Mission (SRTM) 90-m resolution digital elevation data (A. Jarvis et al., Hole-filled seamless SRTM data V4, 2008, http://srtm.csi.cgiar.org). To obtain additional control points along the southwest plateau margin, where marine sediment outcrops are limited, we assumed two different scenarios for the elevation of the paleovalley region. First, we assumed that the paleovalley region was subaerial at the time of marine sediment deposition. Hence, we selected points within the main paleovalleys and defined their elevation to be equal to the closest modern stream elevation in the region. In the second scenario, we assumed that the low-relief surfaces of the horsts were wave-cut platforms during the Late Miocene, and therefore close to sea level. For each scenario, we fit a spline surface to all the points using the Spatial Analyst function in ESRI's ArcMap 9.2. To determine the Late Miocene paleotopography, we subtracted the spline surface from the modern-day SRTM topography plus an additional 50 m, assuming that marine sediments were deposited at 50 m water depth (a reasonable rough estimate based on the facies). We made

Figure 4. Correlation panel of different Upper Miocene stratigraphic sections from the eastern Mediterranean. Numbers in circles show synchronous planktonic foraminifera events recognized both in the Tochni section [*Orszag-Sperber et al.*, 2009] and in the Pissouri Motorway section [*Krijgsman et al.*, 2002]. Letters in circles show either biostratigraphical events recognized in some of the analyzed sections, or a lithologic change that synchronously affected the eastern Mediterranean. The astronomical calibration of the Pissouri section is by *Krijgsman et al.* [2002]. (1) LO of *G. menardii* 4 (7.512 Ma); (2) LO of *G. falconarae* (7.456 Ma); (3) FO of *G. menardii* 5 (7.355 Ma); (4) FRO of the *G. miotumida* group (7.240 Ma); (5) LCO of dominantly sinistral *G. scitula* (7.095 Ma); (6) FO of *G. nicolae* (6.829 Ma); (7) LO of *G. nicolae* (6.722 Ma); (8) LO of the *G. miotumida* group (6.506 Ma); (9) sinistral/dextral coiling change of *Neogloboquadrina acostaensis* (6.337 Ma); (10) first influx (>80%) of sinistral neogloboquadrinids (6.126 Ma). (a_d) disappearance of *Siphonina reticulata* from deep water environments (7.167 Ma [*Kouwenhoven et al.*, 2006]); (a_s) disappearance of *Siphonina reticulata* from shallow water environments (? < 7.167 Ma); (x) LCO of *Sphaeroidinellopsis* spp.; (y) FO of micro-scale laminites in organic-rich marl layers; (z) FCO of *Amaurolithus delicatus* [*Frydas*, 2004]. MES is Messinian Erosional Surface. *Laskar et al.* [1993] insolation in W/m^2.

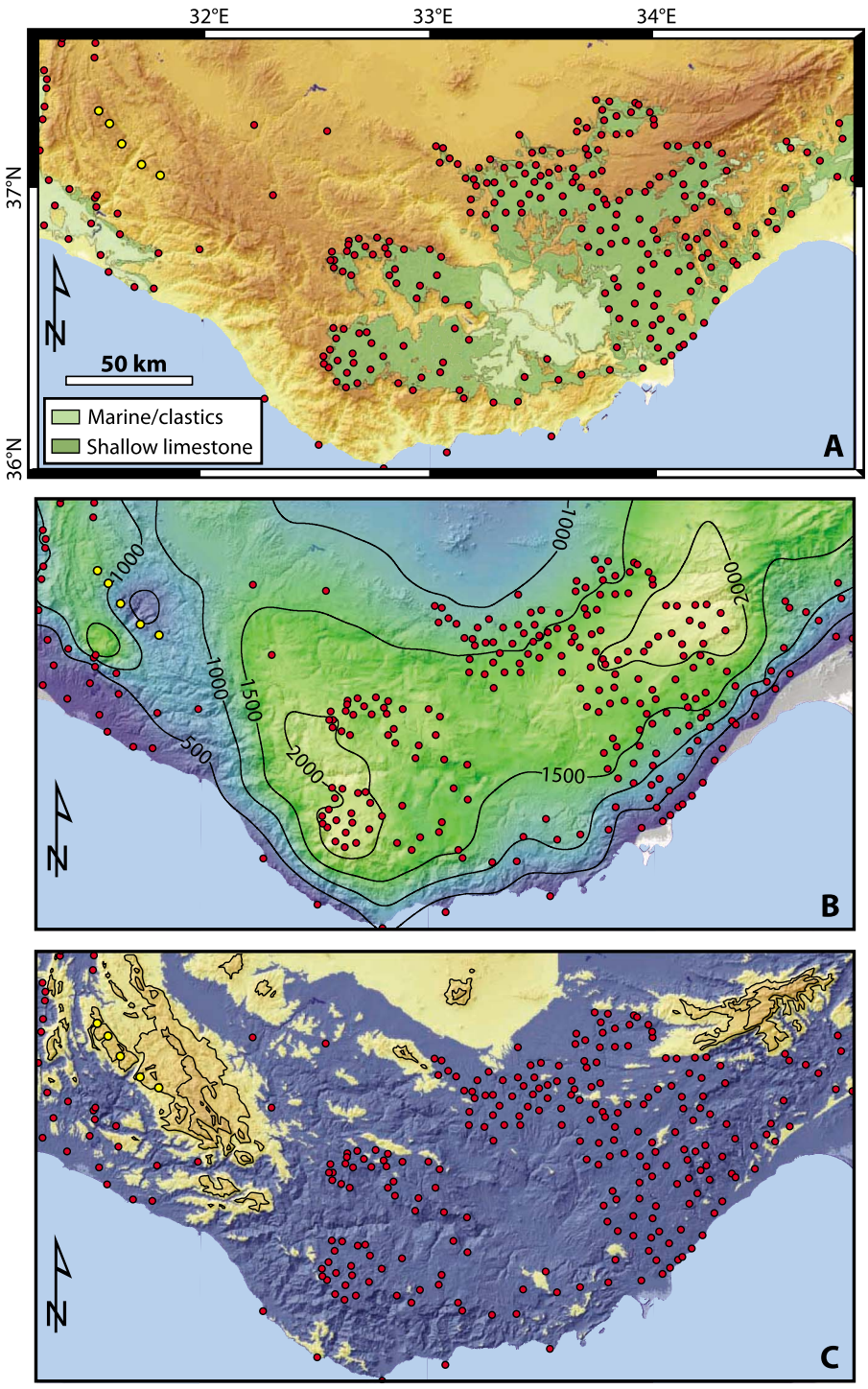

Figure 6. (a) Modern topography with green overlay showing mapped marine sediments. Colored dots are control points used to reconstruct post-Late Miocene uplift pattern. Red dots are points on marine sediments, while yellow dots are in uplifted paleovalleys. (b) Spline fit to control points indicating pattern of surface uplift; contour lines in 500-m intervals. Paleovalleys (yellow points) were assumed to lie at elevations similar to modern rivers in Late Miocene time, while marine sediments (red points) were assumed to lie 50-m below sea level. (c) Paleotopography prior to 7 to 8 Ma, with dark blue regions indicating regions of modern topography that were below sea level prior to 7 to 8 Ma. Contour lines of paleotopography at 500-m intervals.

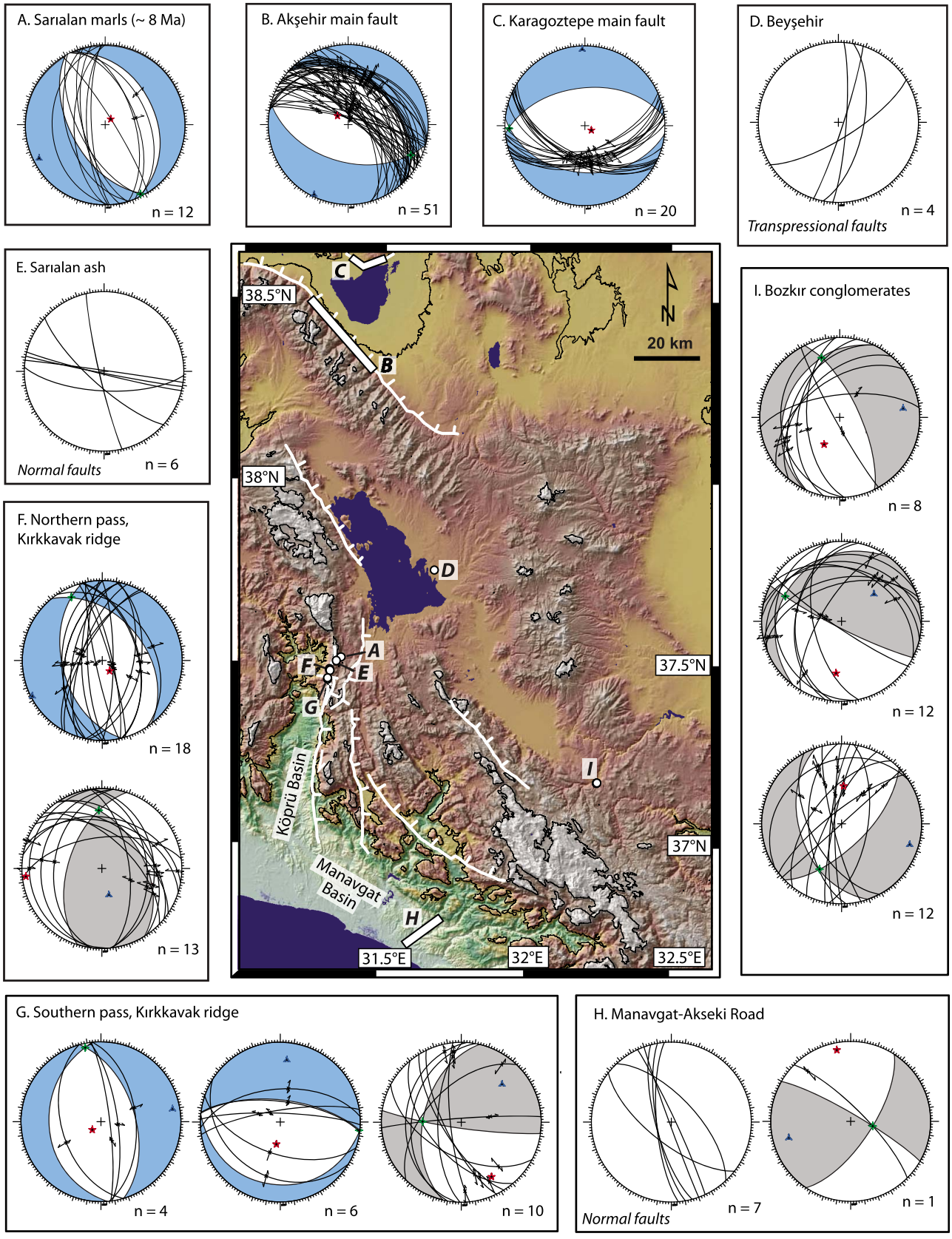
A. Sarıalan marls (~ 8 Ma)
n = 12
B. Akşehir main fault
n = 51
C. Karagoztepe main fault
n = 20
D. Beyşehir
n = 4
Transpressional faults
E. Sarıalan ash
Normal faults
n = 6
F. Northern pass, Kırkkavak ridge
n = 18
n = 13
C
B
A
D
E
F
G
H
I
38.5°N
38°N
37.5°N
37°N
31.5°E
32°E
32.5°E
20 km
N
Köprü Basin
Manavgat Basin
I. Bozkır conglomerates
n = 8
n = 12
n = 12
G. Southern pass, Kırkkavak ridge
n = 4
n = 6
n = 10
H. Manavgat-Akseki Road
Normal faults
n = 7
n = 1

Figure 7

no attempt to correct for post-Late Miocene normal faulting in the paleovalley region or in the Mut Basin.

[33] *Cosentino et al.* [2012b] described post-Late Miocene deformation across the SE plateau margin as a regional asymmetric drape fold. Our reconstruction shows that this deformation pattern is characteristic of the whole southern margin, with uplift magnitudes increasing from the Mediterranean Sea, reaching a broad peak at 1.5 to 2 km magnitude, and dropping to 1 km toward the plateau interior (Figure 6b). The lack of exposed Upper Miocene or younger marine sediments in the plateau interior precludes us from estimating surface uplift farther inland.

[34] Along the southwest plateau margin, cumulative surface uplift reached 1.5 km, with only minor differences in the uplift pattern for our two reconstructed scenarios (Figure 6b and Figure S1 in the auxiliary material).[1] Both reconstructions show that uplift >2 km in magnitude characterizes a broad portion of the S and SE margins, with less uplift of the southwest margin. A trough in the Mut Basin region is likely related to post-Late Miocene normal faulting.

[35] Paleorelief of 1 to 1.5 km appears to have been focused in two regions: one ridge along the Kırkkavak fault (possibly extending through the paleovalley region) at the southwest plateau margin, and a second ridge at the SE plateau margin along the Ecemiş fault zone (Figure 6c). Additional evidence in both regions supports the existence of paleotopographic highs. For example, along the SE margin, marine sediments onlapping the Tauride basement units [*Cosentino et al.*, 2012b] and coarse Oligocene post-alpidic conglomerates along the northern flank of the margin [*Clark and Robertson*, 2002, 2005] imply pre-Late Miocene paleorelief. In the Köprü Basin, along the southwest plateau margin, breccias, alluvial fans, and fan-deltas that abut the Kırkkavak ridge interfinger with Lower and Middle Miocene (Burdigalian-Serravalian) marine sediments [*Deynoux et al.*, 2005; *Çiner et al.*, 2008], implying that a ridge existed since at least Middle Miocene time.

6. Structural and Inferred Tectonic Stress-Field Evolution

[36] Deformation along structures that accompanied surface uplift of the southwest plateau margin is recorded in carbonate rocks and basin fills within the region. Previous workers reported structural and kinematic data from near the southern end of the Kırkkavak fault [*Glover and Robertson*, 1998], the Akşehir graben [*Koçyiğit et al.*, 2000] and from near Tuz Gölü [*Özsayın and Dirik*, 2011]. Our data extend these observations into the plateau margin realm, to better identify the structures that were active during margin uplift.

[1]Auxiliary materials are available in the HTML. doi:10.1029/2011TC003021.

6.1. Methods

[37] We measured macro- and meso-scale fault planes and slickenlines at 6 sites, including the northern end of the Kırkkavak fault (two sites), the Sarıalan section, Beyşehir lake, the Manavgat Basin, and in conglomerates near Bozkır (Figure 7 and Table S1). Using the software Daisy3 (version 4.8.17) [*Salvini et al.*, 1999], we inverted the faults and their kinematic indicators for our sites and for the Akşehir graben data reported by *Koçyiğit et al.* [2000] using the Mohr-Coulomb multiple faulting inversion method to determine the paleostresses associated with the measured population(s). In defining tectonic stress fields, we set a minimum angular distance between populations to be 25 to 35°, a maximum angular scatter between fault conjugates to be twice the minimum angular distance, and a maximum allowable angle among fault systems to be 1.5 standard deviation units. To facilitate comparison of the different deformation phases, we plotted pseudo focal mechanism solutions associated with the principal stress axes as well as the fault planes and kinematic indicators used in the inversions (Figure 7).

[38] Using crosscutting relationships of faults, slickenlines, the age of faulted sediments, and comparison with modern earthquake focal mechanisms from the Harvard global CMT catalog, we identify the changing style of deformation along the plateau margin through time, along with the likely accompanying crustal stress regimes.

6.2. Results

[39] Due to their ubiquity, normal faults have likely played a major role in affecting the modern morphology in the region [e.g., *Monod et al.*, 2006, Figure 2], although nowhere do the fault scarps themselves exceed several hundred meters in relief. Along the northern end of the Kırkkavak fault ridge, two sites within Mesozoic carbonates reveal multiple phases of brittle faulting. At the northern site, crosscutting faults and superimposed slickenlines reveal an earlier phase of E-W contraction with a small left-lateral component. More recent faulting (based on crosscutting relationships) is characterized by WSW-ENE extension. At the southern site (Emerdin Pass), early sinistral transpression is followed by extension that is oriented both E-W and N-S (Figure 7). These observed changes in fault kinematics are similar to descriptions of kinematics by *Dumont and Kerey* [1975] and more recent observations along the southernmost end of the Kırkkavak fault in the Manavgat Basin [*Glover and Robertson*, 1998], who reported that initial shortening was followed by right-lateral, left-lateral, and normal faulting.

[40] East of the Kırkkavak fault ridge, the marls at the base of the Sarıalan section are deformed by high-angle faults. Two kinematic indicators suggest nearly pure dip-slip normal motion associated with NE-SW-directed extension. The "SAR-B" site, which includes the reworked ash, is also cut by high-angle faults that strike approximately E-W to

Figure 7. Psuedo-focal mechanism solutions based on fault inversion modeling at sites throughout the southwest plateau margin. Sites are shown on map with white circles or white bands, and indicate the region across which structural measurements were taken. Plotted fault planes are the population used in defining the associated stress field. Pseudo-focal mechanisms colored blue are interpreted to be younger deformation phases compared to those in gray based on crosscutting relationships of faults or slickenlines. For B and C, blue colors are used because the faults affect sediments of Late Miocene and younger age. Contour lines on topography are at 1000-m intervals (see Figure 2). Late Miocene or younger faults shown in white, with dashes indicating normal movement.

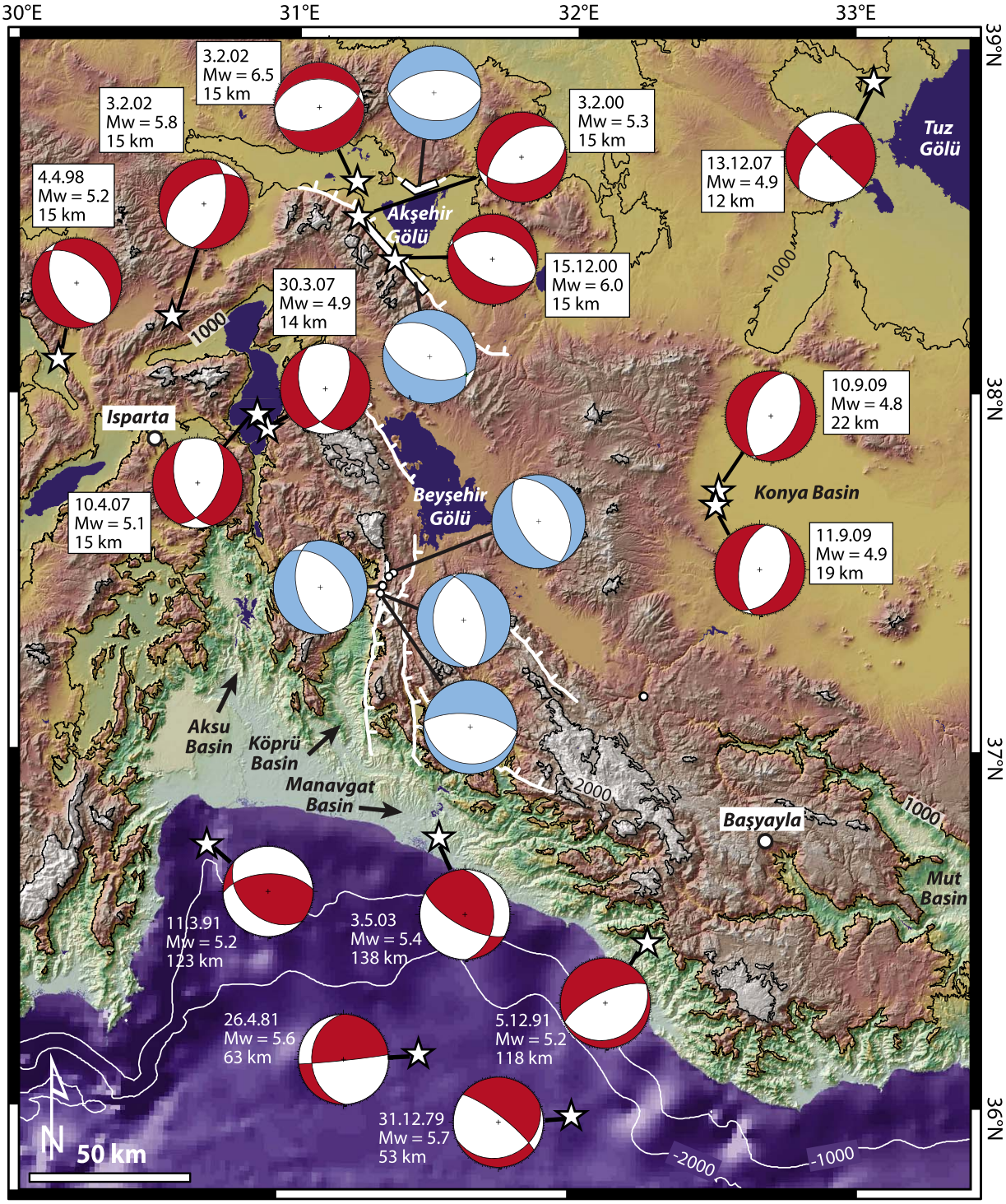

Figure 8. Plot of modern earthquake focal mechanisms (from Figure 1) together with pseudo-focal mechanisms derived from the youngest generation of faults (from Figure 7). Stars indicate epicenters of the earthquakes, while white circles or bands show the region from which fault measurements were collected. Late Miocene or younger faults shown in white, with dashes indicating normal movement.

NW-SE, although no kinematic indicators were identified. These results are similar to the fault kinematic data published by *Koçyiğit et al.* [2000] from the Akşehir graben, which show post-Late Miocene deformation characterized by WNW-ESE and N-S directed extension.

[41] Near Beyşehir, Pliocene lake sediments are cut by high-angle faults with cm-scale offsets that together form a small (ca. 0.5-m wide) positive flower structure. We found no kinematic indicators on the small fault surfaces, although the geometry of the faults implies strike-slip and local transpressional movement.

[42] Within the mapped Oligocene conglomerates close to the town of Bozkır, kinematic indicators reveal sinistral transtension, dextral transtension, and sinsitral transpression, but without clear crosscutting relationships.

[43] In the Manavgat Basin, most faults accommodate normal offsets of the Miocene stratigraphy, but a single kinematic indicator revealed dextral strike-slip motion. Normal faulting likely post-dated strike-slip faulting, as revealed in one transtensional zone that is dragged by a normal fault. Normal faulting also appears to post-date contractional deformation, as the only Early to Middle Miocene units in the basin are affected by folding. *Karabıyıkoğlu et al.* [2000] also reported predominantly normal faulting within the Manavgat Basin.

[44] In summary, several sites (e.g., both sites along Kırkkavak fault ridge, the Akşehir graben sites, and the Manavgat Basin) show that extension post-dated contractional deformation in the southern plateau margin realm. The exclusively extensional structures affecting the ca. 7 to 8 Ma marine sediments near Sarıalan and the Late Miocene and younger sediments in the Akşehir graben and Manavgat Basin limit the end of contractional deformation to before 7 to 8 Ma. Extension was active after deposition of Late Miocene sediments and continued at least through Pliocene time, as evidenced by the faulted Pliocene sediments in the Akşehir region. Growth strata associated with normal faulting in the Akşehir region [*Koçyiğit et al.*, 2000] implies that the extensional phase started as early as Late Miocene time. What role strike-slip motion may have played during this most recent deformation is unclear, but it had at least minor effects on Pliocene-Pleistocene sediments near Beyşehir. Furthermore, despite the lack of a consistent extension direction revealed in the pseudo-focal mechanisms constructed for the youngest generation of faults, we observe a general correspondence between the extension directions of pseudo-focal mechanisms associated with the youngest faults and the focal mechanisms of nearby modern earthquakes (Figure 8).

7. Discussion

7.1. Start of Surface Uplift and Relation to Messinian Draw-Down of Mediterranean

[45] Our new biostratigraphic and lithostratigraphic data from marine sediments along the southwest margin of the Central Anatolian Plateau (Sarıalan section) yield the youngest reported and first Messinian age (ca. 7 Ma) for marine sediments on the uplifted margin. This age is at least 1 Ma younger than the previously reported ages of marine sediments in the region [e.g., *Deynoux et al.*, 2005; *Flecker et al.*, 2005], although those older ages were derived from samples that were ca. 100 m stratigraphically below our highest sample. There are similarities between the biotic assemblage in the basal part of the Sarıalan section with the Başyayla section [*Cosentino et al.*, 2012b], which caps the plateau margin 140 km to the SE. Noting that an additional ca. 100 m of undated marine limestones overlie the Başyayla section [*Cosentino et al.*, 2012b], the youngest marine sediments in that region may also correspond to Messinian ages. Considering that high topography (or active uplift) along the plateau margin is required for the 5.45 Ma onset of >1 km of conglomerate deposition in the Adana Basin [*Cosentino et al.*, 2010], as well as for the onset of conglomerate deposition at a similar time in the offshore Antalya Basin [*Işler et al.*, 2005], our results help to further limit the start of surface uplift throughout the southern plateau margin to between 7 and 5.45 Ma.

[46] Our new data significantly narrow the time window for the start of surface uplift along the plateau margin. The similarity in timing between the start of surface uplift and the ca. 1.5-km lowering of the Mediterranean sea level during the Messinian Salinity Crisis (MSC, 5.96 to 5.33 Ma [*Krijgsman et al.*, 1999]) is compelling, and raises the question of how sea level lowering may have affected the stratigraphic and geomorphic record that we interpret in terms of surface uplift. The return of sea level to pre-MSC conditions at the start of the Pliocene [*Iaccarino et al.*, 1999a, 1999b] implies that Messinian-age marine sediments currently found 1.5 km above sea level can only be related to surface uplift. Less definitive is the effect of sea level lowering on sedimentation within the Adana and Antalya basins. Any relative base level fall can cause river incision [e.g., *Howard*, 1994; *Whipple and Tucker*, 1999, 2002; *Whittaker et al.*, 2007] and increased sediment flux from hillslopes to channels and to depositional basins, often with increased grain sizes in proximal locations [e.g., *Armitage et al.*, 2011; *Whittaker et al.*, 2010]. The varying thickness and nature of sediments deposited during the period of lowered sea level is likely related to the relief and/or tectonic uplift in the surrounding terrestrial areas at the time. For example, the Mondragone 1 well (onshore from the east coast of the Tyrrhenian Basin) reveals 938 m of coarse "Lago-Mare" conglomerates that were deposited in an actively subsiding extensional basin in the back-arc of the Central Apennines [*Cosentino et al.*, 2006]. In contrast, in the tectonically quiescent foreland east of the Central Apennines, the Maiella section shows only a few centimeters of clastic material for the same time interval [*Cosentino et al.*, 2005, 2012a]. The >1 km of conglomerates deposited during just 100 ka in the Adana Basin, and the several hundred meters of conglomerates deposited during a similar time interval in the Antalya Basin, therefore points to significant and/or growing relief along the plateau margin at the time.

[47] Although the full effects of the Messinian sea level lowering on the sedimentary record are unclear, it may have had a lasting imprint on the morphology of the paleovalley region. Hanging valleys in fluvial systems are most commonly created in response to a sudden, rapid increase in uplift rates or drop in base level [*Crosby and Whipple*, 2006; *Wobus et al.*, 2006; *Crosby et al.*, 2007]. A sudden drop in sea level during the MSC could have triggered trunk streams to incise rapidly and abandon their tributaries. Subsequent (or ongoing) uplift would then have helped preserve the morphological signature, since the Zanclean flooding event [*Iaccarino et al.*, 1999a, 1999b], which returned the Mediterranean Sea to its pre-MSC level, may have otherwise induced trunk streams to aggrade to their pre-MSC forms. In this scenario, the hanging tributaries of the paleovalleys would be related to sea level lowering (and perhaps slow background uplift), while the later disruption of the whole network would be associated with km-scale plateau margin uplift.

7.2. Spatial and Temporal Variations in Surface Uplift History

[48] If the hanging tributaries and the paleovalleys reflect a multiphase surface uplift history rather than one partly related to the sea level lowering during the Messinian Salinity Crisis, then the uplift history of the southwest plateau margin may be analogous to one proposed for the Mut region along the S plateau margin. According to *Schildgen et al.* [2012], relatively slow uplift of ca. 0.2 mm/yr in the Mut region starting after 8 Ma preceded faster uplift of 0.6 to 0.7 mm/yr after 1.6 Ma, based on dated uplifted marine sediments and fluvial terraces. The 1.5-km high, 7 Ma marine sediments that we identified yield an average uplift rate of 0.21 mm/yr since 7 Ma. Unfortunately, no younger marine sediments have been identified in the study area, which would allow us to detect changes in uplift rates. The only additional constraints are from the Antalya region, where *Glover and Robertson* [2003] estimated ca. 300-m-high tufa deposits to be 1.5 to 2 Ma, yielding a post-early Pleistocene uplift rate of 0.15 to 0.2 mm/yr. Although those data may imply that uplift rates along the western Central Taurides remained relatively slow, because the tufa deposits are west of the plateau margin, it may not be reasonable to apply those constraints to the southwest margin itself.

[49] Despite the lack of information on the more recent uplift history for the southwest margin of the Central Anatolian Plateau, the similarity of the long-term surface uplift rates along the southwest margin to the average 8 Ma to 1.6 Ma uplift rates along the S and SE margins could imply that the mechanisms driving uplift in both regions were similar until 1.6 Ma, after which other processes increased the uplift rate along the S and SE margins. This interpretation is supported by the spatial pattern of uplift, which generally reaches maximum values of ca. 1.5 km along the southwest margin compared to >2 km along the S and SE margin.

7.3. Changes in Tectonic Stress Regime and Associated Uplift Mechanisms

[50] The early compressional tectonic stress regime along the southwest margin appears to have ended prior to ca. 7 to 8 Ma based on lack of folding or thrust faulting in the Late Miocene sediments of the Sarıalan section, in the Akşehir graben [*Koçyiğit et al.*, 2000], and in the Manavgat Basin. Reverse faults and low-angle thrusts along the Kırkkavak ridge, which is a region that formed a paleotopographic high prior to 7 to 8 Ma, indicate that early topography in the area may have developed due to crustal shortening. The structure with a similar orientation along the western margin of the Akşehir graben similarly shows contraction prior to Late Miocene time [*Koçyiğit et al.*, 2000]. The shortening that created the initial topography may have been associated with westward extrusion of the Anatolian microplate starting at ca. 11 Ma [*Şengör et al.*, 2005], as both structures lie nearly perpendicular to the extrusion direction. Alternatively, the shortening could have been related to tightening of the Isparta Angle [e.g., *Kissel and Poisson*, 1986; *Morris and Robertson*, 1993; *Kissel et al.*, 1993; *van Hinsbergen et al.*, 2010]. Later, CCW rotation of Central Anatolia may have induced crustal shortening along the S-SE plateau margin and strike-slip motion along the southwest margin, but no contractional structures that were active after 7 to 8 Ma have been identified along the S-SE plateau margin. The shortening zone imaged in the offshore Antalya Basin (which appears to align with the Aksu Basin and the Kyrenia range of northern Cyprus, as noted by *Poisson et al.* [2003]) could be associated with either CCW rotation and/or with contraction in the hanging wall above the subducting Cyprus slab. The post-Late Miocene topography created along that contractional zone, however, is minimal compared to the km-scale, post-7 Ma uplift of the southern plateau margin. As a result, any surface uplift related to horizontal plate motions (including westward extrusion of Anatolia, CCW rotation of Central Anatolia, or modern subduction) could help explain the existence of paleotopography prior to 7 Ma along the southwest margin, minor topographic relief developed after Miocene time south of the plateau, and possibly a change from contraction to strike-slip deformation along the Kırkkavak fault. Horizontal motions cannot, however, explain post-7 Ma uplift of the southern plateau margin.

[51] Mechanisms responsible for the later crustal extension must also allow for surface uplift at a similar time. Heating at the base of the crust is a likely scenario, as the resulting thermally driven isostatic uplift may induce normal faulting [e.g., *Davies and von Blanckenburg*, 1995; *Duretz et al.*, 2011; *Göğüş and Pysklywec*, 2008]. The long-wavelength warping that would result from such a deep-seated mechanism could induce km-scale uplift, but because differential uplift could be at least partly accommodated by tilting or warping of the crust, individual faults may only show offsets of several hundred meters or less. The orientation of extension is also unlikely to be systematic on a regional scale, as the direction would largely depend on the geometry of the buoyant region at depth. Asthenospheric upwelling following lithospheric delamination, slab break-off, and slab tearing are consistent with both the magnitude of surface uplift, the structures related to a tensional stress regime, and the general lack of a consistent extension direction.

[52] The pattern of post-7 Ma uplift, together with constraints on the geometry of the modern subducting slabs, can help clarify which processes were likely to have induced uplift and upper crustal extension. Higher cumulative uplift has occurred along the S and SE plateau margin compared to the southwest margin. As suggested by *Cosentino et al.* [2012b], the absence of a subducting slab east of Cyprus based on P wave tomography implies that uplift of the S and SE margin could be related to slab break-off. Slab break-off seems less likely to explain uplift farther west between Cyprus and the Isparta Angle, as both P wave tomography [*Biryol et al.*, 2011; *Gans et al.*, 2009] and seismic and gravity data [*Kalyoncuoğlu et al.*, 2011] support ongoing subduction. Alternatively in that region, a tear between the Aegean and Cyprus slabs may allow asthenospheric upwelling that heats the overriding plate (Figure 9). The ca. 4 to 4.7 Ma alkaline volcanic rocks at the northern end of the Isparta Angle, interpreted by some authors to indicate upwelling asthenosphere through a slab tear [*Francalanci et al.*, 2000; *Dilek and Altunkaynak*, 2009; *Dilek and Sandvol*, 2009], support our interpretation that a slab tear could be related to the onset of both the extensional regime and surface uplift along the southwest margin, particularly considering that the Pliocene volcanic ages represent a younger limit to the start of slab tearing. Lithospheric

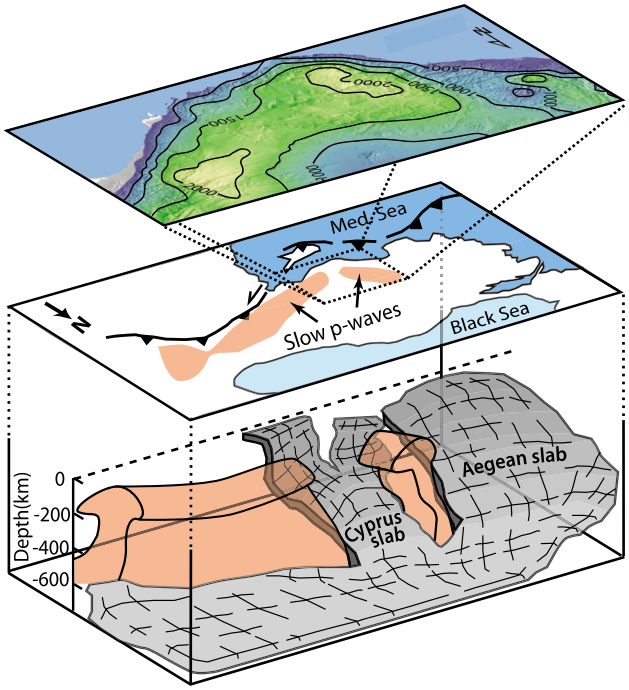

Figure 9. Schematic illustration of upwelling asthenosphere through lithospheric slab break and tear (geometry of slabs from *Biryol et al.* [2011], with map above showing regions of low Pn-wave velocities in pink [*Biryol et al.*, 2011; *Gans et al.*, 2009]). Upper map shows reconstructed, contoured map of surface uplift (as in Figure 6b). Note the general similarity between the pattern of surface uplift and low P wave velocities, which are consistent with the suspected pattern of upwelling asthenosphere.

delamination may still be a possible explanation for uplift along the southwest margin, but without additional constraints on uplift from the plateau interior, it is difficult to assess whether or not it is necessary to invoke a mechanism capable of generating uplift over a broader region.

8. Conclusions

[53] Our new biostratigraphic data from 1.5-km high marine sediments along the southwest margin of the Central Anatolian Plateau (western Central Taurides) limit the age of the highest sediments to <7.17 Ma, while regional lithostratigraphic correlations imply that the age is <6.7 Ma. The implied post-7 Ma uplift along the southwest margin is broadly coeval with the start of uplift along the S and SE plateau margins, as shown by ca. 8 Ma marine sediments uplifted to ca. 2 km elevation near the town of Başyayla [*Cosentino et al.*, 2012b]. Together with the Late Miocene onset of coarse conglomerate deposition in the bordering Adana and Antalya basins [*Işler et al.*, 2005; *Cosentino et al.*, 2010], and along the northern flank of the southern plateau margin starting in Late Miocene to Pliocene time [*Jaffey and Robertson*, 2005], the data imply that 1.5 to 2 km of surface uplift along the southern margin of the Central Anatolian plateau started between ca. 7 and 5.45 Ma.

[54] The tectonic stress regime affecting the southwest plateau margin appears to have changed sometime after ca. 8 Ma from compression to tension/transtension, as shown by widespread occurrence of normal and strike-slip faults in Upper Miocene and younger sediments. These faults, together with tensional/transtensional upper crustal earthquake focal mechanisms, attest to a change in the tectonic stress field and a changeover of deformation styles coeval with surface uplift. Considering also (1) ca. 4 to 4.7 Ma alkaline volcanic units at the northern end of the Isparta Angle associated with extension and possibly linked to upwelling asthenosphere [*Francalanci et al.*, 2000; *Dilek and Altunkaynak*, 2009; *Dilek and Sandvol*, 2009], (2) P wave tomography data suggesting the existence of a slab tear beneath the southwest plateau margin [*Biryol et al.*, 2011], and (3) the pattern of uplift focused along the modern plateau margin, one plausible mechanism for surface uplift is asthenospheric upwelling through a slab tear that started beneath the plateau margin between ca. 7 and 5 Ma (Figure 9). Better constraints on uplift in the plateau interior are necessary to assess whether or not processes that can induce uplift over a broader region, such as lithospheric delamination, may have induced to uplift along the southwest margin of the plateau. Although regional tectonic plate movements may have contributed to the development of early topographic growth in the region through crustal shortening prior to 7 Ma, the most recent surface uplift along the southwest plateau margin, and probably along the entire southern plateau margin of Central and Eastern Anatolia, may be primarily explained by slab dynamics and upper mantle upwelling.

[55] **Acknowledgments.** This work is part of the Vertical Anatolian Movements Project (VAMP), funded by the TOPO-EUROPE initiative of the European Science Foundation, including contributions by the IGAG-CNR (com. TA.P05.009, mod. TA.P05.009.003) and the German Science Foundation (DFG: STR373/25–1; EC 138/5–1). Schildgen was supported by the Leibniz Center for Surface Processes and Climate Studies at the University of Potsdam (DFG: STR373/20–1) and the Alexander von Humboldt Foundation. We thank Paolo Ballato and Daniel Melnick for discussions. We also thank Erkan Aydar and Attila Çiner for logistical help and valuable discussions of the regional geology, and Neslihan Üdal and Erdal Kosun for help with field work. Aral Okay and an anonymous reviewer provided helpful comments that improved the manuscript.

References

Akay, E., and S. Uysal (1985), Orta torosların batısındaki (Antalya) Neojen çökellerinin stratigrafisi, sedimentolojisi ve yapısal jeolojisi, report, Maden Tetkik ve Arama Genel Müdürlüğü, Ankara.

Akay, E., S. Uysal, A. Poisson, J. Cravatte, and C. Müller (1985), Stratigraphy of the Antalya Neogene Basin, *Bull. Geol. Soc. Turk.*, *28*, 105–119.

Aksu, A. E., T. J. Calon, J. Hall, S. Mansfield, and D. Yaşar (2005), The Cilicia-Adana basin complex, Eastern Mediterranean: Neogene evolution of an active fore-arc basin in an obliquely convergent margin, *Mar. Geol.*, *221*, 121–159, doi:10.1016/j.margeo.2005.03.011.

Alıcı, P., A. Temel, A. Gourgaud, G. Kieffer, and M. N. Gündoğdu (1998), Petrology and geochemistry of potassic rocks in the Gölcük area (Isparta, SW Turkey): Genesis of enriched alkaline magmas, *J. Volcanol. Geotherm. Res.*, *85*(1–4), 423–446, doi:10.1016/S0377-0273(98)00065-1.

Allmendinger, R. W., T. E. Jordan, S. M. Kay, and B. L. Isacks (1997), The evolution of the Altiplano-Puna plateau in the Central Andes, *Annu. Rev. Earth Planet. Sci.*, *25*, 139–174, doi:10.1146/annurev.earth.25.1.139.

Altunkaynak, Ş., and Y. Dilek (2006), Timing and nature of postcollisional volcanism in western Anatolia and geodynamic implications, in *Post-Collisional Tectonics and Magmatism of the Eastern Mediterranean Region*, edited by Y. Dilek and S. Pavlides, *Spec. Pap. Geol. Soc. Am.*, *409*, 321–351.

Armitage, J. J., R. A. Duller, A. C. Whittaker, and P. A. Allen (2011), Transformation of tectonic and climatic signals from source to sedimentary archive, *Nat. Geosci.*, *4*(4), 231–235, doi:10.1038/ngeo1087.

Barka, A., and R. Reilinger (1997), Active tectonics of the Mediterranean region: Deduced from GPS, neotectonic and seismicity data, *Ann. Geofis.*, *XL*, 587–610.

Basang, C., F. J. Eckard, W. Harre, H. Kreuzer, and P. Müller (1977), Radiometrische Altersbestimmungen an neogenen Eruptivgesteinen der Türkei, *Geol. J.*, *25*, 3–36.

Bellanca, A., A. Caruso, F. Ferruzza, R. Neri, J. M. Rouchy, M. Sprovieri, and M.-M. Blanc-Valleron (2001), Sedimentary record of the transition from marine to hypersaline conditions in the Messinian Tripoli Formation in the marginal areas of the Sicilian Basin, *Sediment. Geol.*, *140*(1–2), 87–105, doi:10.1016/S0037-0738(00)00173-1.

Biryol, C. B., S. L. Beck, G. Zandt, and A. A. Özacar (2011), Segmented African lithosphere beneath the Anatolian region inferred from teleseismic *P*-wave tomography, *Geophys. J. Int.*, *184*, 1037–1057, doi:10.1111/j.1365-246X.2010.04910.x.

Bizon, G., B. Biju-Duval, J. Letousey, O. Monod, A. Poisson, B. Özer, and E. Öztümer (1974), Nouvelles précision stratigraphiques concernant les basin tertiaires du sud de la Turquie (Antalya, Mut, Adana), *Rev. Inst. Fr. Pet.*, *29*, 305–320.

Blisniuk, P. M., and L. A. Stern (2005), Stable isotope paleoaltimetry: A critical review, *Am. J. Sci.*, *305*(10), 1033–1074, doi:10.2475/ajs.305.10.1033.

Blumenthal, M. M. (1963), Le systéme structural du Taurus sud Anatolies, in *Livre à Mémoire de Professor P. Fallot*, *Mem. Soc. Geol. Fr.*, vol. 2, edited by M. D. Delga, pp. 611–662, Soc. Geol. Fr., Paris.

Bowring, J. F., N. M. McLean, and S. A. Bowring (2011), Engineering cyber infrastructure for U-Pb geochronology: Tripoli and U-Pb_Redux, *Geochem. Geophys. Geosyst.*, *12*, Q0AA19, doi:10.1029/2010GC003479.

Burton-Ferguson, R., A. E. Aksu, T. J. Calon, and J. Hall (2005), Seismic stratigraphy and structural evolution of the Adana Basin, eastern Mediterranean, *Mar. Geol.*, *221*, 189–222, doi:10.1016/j.margeo.2005.03.009.

Çiner, A., M. Karabıyıkoğlu, O. Monod, M. Deynoux, and S. Tuzcu (2008), Late Cenozoic sedimentary evolution of the Antalya Basin, southern Turkey, *Turk. J. Earth Sci.*, *17*, 1–41.

Clark, M. S., and A. H. F. Robertson (2002), The role of the Early Tertiary Ulukişla Basin, southern Turkey in suturing of the Mesozoic Tethys ocean, *J. Geol. Soc.*, *159*, 673–690, doi:10.1144/0016-764902-015.

Clark, M., and A. H. F. Robertson (2005), Uppermost Cretaceous-Lower Tertiary Ulukişla Basin, south-central Turkey: Sedimentary evolution of part of a unified basin complex within an evolving Neotethyan suture zone, *Sediment. Geol.*, *173*, 15–51, doi:10.1016/j.sedgeo.2003.12.010.

Cosentino, D., P. Cipollari, S. Lo Mastro, and C. Giampaolo (2005), High-frequency cyclicity in the latest Messinian Adriatic foreland basin: Insight into palaeoclimate and palaeoenvironments of the Mediterranean *Lago-Mare* episode, *Sediment. Geol.*, *178*(1–2), 31–53, doi:10.1016/j.sedgeo.2005.03.010.

Cosentino, D., H. Federici, P. Cipollari, and E. Gliozzi (2006), Environments and tectonic instability in central Italy (Garigliano Basin) during the late Messinian Lago-Mare episode: New data from the onshore Mondragone 1 well, *Sediment. Geol.*, *188–189*, 297–317, doi:10.1016/j.sedgeo.2006.03.010.

Cosentino, D., G. Darbaş, E. Gliozzi, F. Grossi, K. Gürbüz, and A. Nazik (2010), How did the Messinian Salinity Crisis impact the Adana Basin?, paper presented at 7th International Symposium on Eastern Mediterranean Geology, Univ. of Cukurova, Adana, Turkey, 18–22 Oct.

Cosentino, D., A. Bertini, P. Cipollari, F. Florindo, E. Gliozzi, F. Grossi, S. Lo Mastro, and M. Sprovieri (2012a), Orbitally forced palaeoenvironmental and palaeoclimate changes in the late post-evaporitic Messinian of the central Mediterranean Basin, *Geol. Soc. Am. Bull.*, doi:10.1130/B30462.1, in press.

Cosentino, D., T. F. Schildgen, P. Cipollari, C. Faranda, E. Gliozzi, N. Hudáčková, S. Lucifora, and M. R. Strecker (2012b), Late Miocene surface uplift of the southern margin of the Central Anatolian plateau, Central Taurides, Turkey, *Geol. Soc. Am. Bull.*, *124*, 133–145, doi:10.1130/B30466.1.

Crosby, B. T., and K. X. Whipple (2006), Knickpoint initiation and distribution within fluvial networks: 236 waterfalls in the Waipaoa River, North Island, New Zealand, *Geomorphology*, *82*, 16–38, doi:10.1016/j.geomorph.2005.08.023.

Crosby, B. T., K. X. Whipple, N. M. Gasparini, and C. W. Wobus (2007), Formation of fluvial hanging valleys: Theory and simulation, *J. Geophys. Res.*, *112*, F03S10, doi:10.1029/2006JF000566.

Darbaş, G., and A. Nazik (2010), Micropaleontology and paleoecology of the Neogene sediments in the Adana Basin (South of Turkey), *J. Asian Earth Sci.*, *39*, 136–147, doi:10.1016/j.jseaes.2010.03.002.

Davies, J. H., and F. von Blanckenburg (1995), Slab breakoff–A model of lithosphere detachment and its test in the magmatism and deformation of collisional orogens, *Earth Planet. Sci. Lett.*, *129*(1–4), 85–102, doi:10.1016/0012-821X(94)00237-S.

Deynoux, M., A. Çiner, O. Monod, M. Karabıyıkoğlu, G. Manatschal, and S. Tuzcu (2005), Facies architecture and depositional evolution of alluvial fan to fan-delta complexes in the tectonically active Miocene Köprüçay Basin, Isparta Angle, Turkey, *Sediment. Geol.*, *173*, 315–343, doi:10.1016/j.sedgeo.2003.12.013.

Di Stefano, E., M. B. Cita, S. Spezzaferri, and R. Sprovieri (1999), The Messinian-Zanclean Pissouri Section (Cyprus, eastern Mediterranean), *Mem. Soc. Geol. Ital.*, *118*, 133–144.

Dilek, Y., and Ş. Altunkaynak (2009), Geochemical and temporal evolution of Cenozoic magmatism in western Turkey: Mantle response to collision, slab break-off, and lithospheric tearing in an orogenic belt, in *Collision and Collapse at the Africa-Arabia-Eurasia Subduction Zone*, edited by D. J. J. van Hinsbergen, M. A. Edwards, and R. Govers, *Geol. Soc. Spec. Publ.*, *311*, 213–233, doi:10.1144/SP311.8.

Dilek, Y., and E. Sandvol (2009), Seismic structure, crustal architecture and tectonic evolution of the Anatolian-African plate boundary and the Cenozoic orogenic belts in the Eastern Mediterranean region, in *Ancient Orogens and Modern Analogues*, edited by J. B. Murphy, J. D. Keppie, and A. J. Hynes, *Geol. Soc. Spec. Publ.*, *327*, 127–160, doi:10.1144/SP327.8.

Dumont, J.-F., and E. Kerey (1975), L'accident de Kırkkavak, un decrochement majeur dans le Taurus occidental (Turquie), *Bull. Soc. Geol. Fr.*, *16*, 1071–1073.

Duretz, T., T. V. Gerya, and D. A. May (2011), Numerical modelling of spontaneous slab breakoff and subsequent topographic response, *Tectonophysics*, *502*, 244–256, doi:10.1016/j.tecto.2010.05.024.

England, P., and G. Houseman (1989), Extension during continental convergence, with application to the Tibetan Plateau, *J. Geophys. Res.*, *94*(B12), 17,561–17,579, doi:10.1029/JB094iB12p17561.

Faranda, C., P. Cipollari, D. Cosentino, E. Gliozzi, and G. Pipponzi (2008), Late Miocene ostracod assemblages from eastern Mediterranean coral-reef complexes (central Crete, Greece), *Rev. Micropaleontol.*, *51*, 287–308, doi:10.1016/j.revmic.2007.06.002.

Flecker, R., A. H. F. Robertson, A. Poisson, and C. Müller (1995), Facies and tectonic significance of two contrasting Miocene basins in south coastal Turkey, *Terra Nova*, *7*(2), 221–232, doi:10.1111/j.1365-3121.1995.tb00691.x.

Flecker, R., R. M. Ellam, C. Müller, A. Poisson, A. H. F. Robertson, and J. Turner (1998), Application of Sr isotope stratigraphy and sedimentary analyses to the origin and evolution of the Neogene basins in the Isparta Angle, southern Turkey, *Tectonophysics*, *298*, 83–101, doi:10.1016/S0040-1951(98)00179-6.

Flecker, R., A. Poisson, and A. H. F. Robertson (2005), Facies and palaeogeographic evidence for the Miocene evolution of the Isparta Angle in its regional eastern Mediterranean context, *Sediment. Geol.*, *173*(1–4), 277–314, doi:10.1016/j.sedgeo.2003.10.014.

Francalanci, L., F. Innocenti, P. Manetti, and M. Y. Savasçın (2000), Neogene alkaline volcanism of the Afyon-Isparta area, Turkey: Petrogenesis and geodynamic implications, *Mineral. Petrol.*, *70*, 285–312, doi:10.1007/s007100070007.

Frizon de Lamotte, D., A. Poisson, C. Aubourg, and H. Temiz (1995), Chevauchements post-Tortonien ver l'Ouest puis vers le Sud au coeur de l'Angle d'Isparta (Taurus, Turquie). Conséquences géodynamiques, *Bull. Soc. Geol. Fr.*, *166*, 59–67.

Frydas, D. (2004), Calcareous and siliceous phytoplankton stratigraphy of Neogene marine sediments in central Crete (Greece), *Rev. Micropaleontol.*, *47*, 87–102, doi:10.1016/j.revmic.2004.03.002.

Gans, C. R., S. L. Beck, G. Zandt, C. B. Biryol, and A. A. Özacar (2009), Detecting the limit of slab break-off in central Turkey: New high-resolution Pn tomography results, *Geophys. J. Int.*, *179*(3), 1566–1572, doi:10.1111/j.1365-246X.2009.04389.x.

Gerstenberger, H., and G. Haase (1997), A highly effective emitter substance for mass spectrometric Pb isotope ratio determinations, *Chem. Geol.*, *136*(3–4), 309–312, doi:10.1016/S0009-2541(96)00033-2.

Glover, C., and A. Robertson (1998), Neotectonic intersection of the Aegean and Cyprus tectonic arcs: Extensional and strike-slip faulting in the Isparta Angle, SW Turkey, *Tectonophysics*, *298*, 103–132, doi:10.1016/S0040-1951(98)00180-2.

Glover, C., and A. H. F. Robertson (2003), Origin of tufa (cool-water carbonate) and related terraces in the Antalya area, SW Turkey, *Geol. J.*, *38*(3–4), 329–358, doi:10.1002/gj.959.

Göğüş, O. H., and R. N. Pysklywec (2008), Mantle lithosphere delamination driving plateau uplift and synconvergent extension in eastern Anatolia, *Geology*, *36*(9), 723–726, doi:10.1130/G24982A.1.

Gürbüz, K., and G. Kelling (1993), Provenance of Miocene submarine fans in the northern Adana Basin, southern Turkey: A test of discriminant function analysis, *Geol. J.*, *28*, 277–293, doi:10.1002/gj.3350280307.

Harrison, R., et al. (2008), Bedrock geologic map of the Greater Lefkosia area, Cyprus, with explanatory text, scale 1:25,000, *U.S. Geol. Surv. Sci. Invest. Map*, *3046*, 36 pp.

Hilgen, F. J., W. Krijgsman, C. G. Langereis, L. J. Lourens, A. Santarelli, and W. J. Zachariasse (1995), Extending the astronomical (polarity) time scale into the Miocene, *Earth Planet. Sci. Lett.*, *136*, 495–510, doi:10.1016/0012-821X(95)00207-S.

Hilley, G. E., and M. R. Strecker (2004), Steady state erosion of critical Coulomb wedges with applications to Taiwan and the Himalaya, *J. Geophys. Res.*, *109*, B01411, doi:10.1029/2002JB002284.

Howard, A. (1994), A detachment-limited model of drainage basin evolution, *Water Resour. Res.*, *30*, 2261–2285, doi:10.1029/94WR00757.

Hüsing, S. K., K. F. Kuiper, W. Link, F. J. Hilgen, and W. Krijgsman (2009), The upper Tortonian-lower Messinian at Monte dei Corvi (Northern Apennines, Italy): Completing a Mediterranean reference section for the Tortonian Stage, *Earth Planet. Sci. Lett.*, *282*, 140–157, doi:10.1016/j.epsl.2009.03.010.

Iaccarino, S., D. Castradori, M. B. Cita, E. Di Stefano, S. Gaboardi, J. A. McKenzie, S. Spezzaferri, and R. Sprovieri (1999a), The Miocene-Pliocene boundary and the significance of the earliest Pliocene flooding in the Mediterranean, *Mem. Soc. Geol. Ital.*, *54*, 109–131.

Iaccarino, S., M. B. Cita, S. Gaboardi, and G. M. Gruppini (1999b), High-resolution biostratigraphy at the Miocene/Pliocene boundary in holes 974B and 975B, western Mediterranean, in *Mediterranean II—The Western Mediterranean*, edited by R. Zahn, M. C. Comas, and A. Klaus, *Proc. Ocean Drill. Prog. Sci. Results*, *161*, 197–221.

Işler, F. I., A. E. Aksu, J. Hall, T. J. Calon, and D. Yaşar (2005), Neogene development of the Antalya Basin, Eastern Mediterranean: An active forearc basin adjacent to an arc junction, *Mar. Geol.*, *221*, 299–330, doi:10.1016/j.margeo.2005.03.006.

Jackson, J. (1992), Partitioning of strike-slip and convergent motion between Eurasia and Arabia in eastern Turkey, *J. Geophys. Res.*, *97*, 12,471–12,479, doi:10.1029/92JB00944.

Jackson, J., and D. McKenzie (1984), Active tectonics of the Alpine-Himalayan belt between western Turkey and Pakistan, *Geophys. J. R. Astron. Soc.*, *77*(1), 185–246, doi:10.1111/j.1365-246X.1984.tb01931.x.

Jaffey, A. H., K. F. Flynn, L. E. Glendenin, W. C. Bentley, and A. M. Essling (1971), Precision measurement of half-lives and specific activities of 235U and 238U, *Phys. Rev. C*, *4*, 1889–1906, doi:10.1103/PhysRevC.4.1889.

Jaffey, N., and A. Robertson (2005), Non-marine sedimentation associated with Oligocene-Recent exhumation and uplift of the Central Taurus Mountains, S Turkey, *Sediment. Geol.*, *173*, 53–89, doi:10.1016/j.sedgeo.2003.11.025.

Kalyoncuoğlu, Ü. Y., Ö. Elitok, M. N. Dolmaz, and N. C. Anadolu (2011), Geophysical and geological imprints of southern Neotethyan subduction between Cyprus and the Isparta Angle, SW Turkey, *J. Geodyn.*, *52*, 70–82, doi:10.1016/j.jog.2010.12.001.

Karabıyıkoğlu, M., A. Çiner, O. Monod, M. Deynoux, S. Tuzcu, and S. Örçen (2000), Tectonosedimentary evolution of the Miocene Manavgat Basin, western Taurides, Turkey, in *Tectonics and Magmatism in Turkey and the Surrounding Area*, edited by E. Bozkurt, J. A. Winchester, and J. D. A. Piper, *Geol. Soc. Spec. Publ.*, *173*, 271–294, doi:10.1144/GSL.SP.2000.173.01.14.

Kay, R. W., and S. M. Kay (1993), Delamination and delamination magmatism, *Tectonophysics*, *219*(1–3), 177–189, doi:10.1016/0040-1951(93)90295-U.

Keskin, M. (2003), Magma generation by slab steepening and breakoff beneath a subduction accretion complex: An alternative model for collision-related volcanism in Eastern Anatolia, Turkey, *Geophys. Res. Lett.*, *30*(24), 8046, doi:10.1029/2003GL018019.

Kissel, C., and A. Poisson (1986), Étude paleomagnetique préliminaire des formations Cenozoiques des Bey Dağları (Taurides occidentales-Turquie), *C. R. Acad. Sci. Ser. II*, *302*, 343–348.

Kissel, C., O. Averbuch, D. Frizon de Lamotte, O. Monod, and S. Allerton (1993), First palaeomagnetic evidence of a post-Eocene clockwise rotation of the Western Taurus thrust belt, east of the Isparta reentrant (southwestern Turkey), *Earth Planet. Sci. Lett.*, *117*, 1–14, doi:10.1016/0012-821X(93)90113-N.

Koçyiğit, A., E. Ünay, and G. Saraç (2000), Episodic graben formation and extensional neotectonic regime in west Central Anatolia and the Isparta Angle: A case study in the Akşehir-Afyon Graben, Turkey, in *Tectonics and Magmatism in Turkey and the Surrounding Area*, edited by E. Bozkurt, J. A. Winchester, and J. D. A. Piper, *Geol. Soc. Spec. Publ.*, *173*, 405–421.

Kouwenhoven, T. J., M.-S. Seidenkrantz, and G. J. van der Zwaan (1999), Deep-water changes: The near-synchronous disappearance of a group of benthic foraminifera from the late Miocene Mediterranean, *Palaeogeogr. Palaeoclimatol. Palaeoecol.*, *152*, 259–281, doi:10.1016/S0031-0182(99)00065-6.

Kouwenhoven, T. J., F. J. Hilgen, and G. J. van der Zwaan (2003), Late Tortonian–early Messinian stepwise disruption of the Mediterranean–Atlantic connections: Constraints from benthic foraminiferal and geochemical data, *Palaeogeogr. Palaeoclimatol. Palaeoecol.*, *198*, 303–319, doi:10.1016/S0031-0182(03)00472-3.

Kouwenhoven, T. J., C. Morigi, A. Negri, S. Giunta, W. Krijgsman, and J.-M. Rouchy (2006), Paleoenvironmental evolution of the eastern Mediterranean during the Messinian: Constraints from integrated microfossil data of the Pissouri basin (Cyprus), *Mar. Micropaleontol.*, *60*, 17–44, doi:10.1016/j.marmicro.2006.02.005.

Krijgsman, W., F. J. Hilgen, C. G. Langereis, A. Santarelli, and W. J. Zachariasse (1995), Late Miocene magnetostratigraphy, biostratigraphy and cyclostratigraphy in the Mediterranean, *Earth Planet. Sci. Lett.*, *136*, 475–494, doi:10.1016/0012-821X(95)00206-R.

Krijgsman, W., F. J. Hilgen, I. Raffi, F. J. Sierro, and D. S. Wilson (1999), Chronology, causes and progression of the Messinian salinity crisis, *Nature*, *400*, 652–655, doi:10.1038/23231.

Krijgsman, W., M.-M. Blanc-Valleron, R. Flecker, F. J. Hilgen, T. J. Kouwenhoven, D. Merle, F. Orszag-Sperber, and J.-M. Rouchy (2002), The onset of the Messinian salinity crisis in the Eastern Mediterranean (Pissouri Basin, Cyprus), *Earth Planet. Sci. Lett.*, *194*, 299–310, doi:10.1016/S0012-821X(01)00574-X.

Laskar, L. J., F. Joutel, and F. Boudin (1993), Orbital, precessional, and insolation quantities for the Earth from −20 Myr to +10 Myr, *Astron. Astrophys.*, *270*, 522–533.

Le Pichon, X., and J. Angelier (1979), The Hellenic arc and trench system: A key to the neotectonic evolution of the eastern Mediterranean area, *Tectonophysics*, *60*, 1–42, doi:10.1016/0040-1951(79)90131-8.

Lefèvre, C., H. Bellon, and A. Poisson (1983), Présence de leucitites dans le volcanism Pliocène de la region d'Isparta (Taurides Occidentales, Turquie), *C. R. Acad. Sci. Paris*, *297*, 367–372.

Lenters, J. D., and K. H. Cook (1997), On the origin of the Bolivian high and related circulation features of the South American climate, *J. Atmos. Sci.*, *54*, 656–678, doi:10.1175/1520-0469(1997)054<0656:OTOOTB>2.0.CO;2.

Mattinson, J. M. (2005), Zircon U-Pb chemical abrasion ("CA-TIMS") method: Combined annealing and multi-step partial dissolution analysis for improved precision and accuracy of zircon ages, *Chem. Geol.*, *220*(1–2), 47–66, doi:10.1016/j.chemgeo.2005.03.011.

McClusky, S., et al. (2000), Global Positioning System constraints on plate kinematics and dynamics in the eastern Mediterranean and Caucasus, *J. Geophys. Res.*, *105*, 5695–5719, doi:10.1029/1999JB900351.

McKenzie, D. P. (1970), Plate tectonics of the Mediterranean region, *Nature*, *226*, 239–243, doi:10.1038/226239a0.

McKenzie, D. (1978), Active tectonics of the Alpine-Himalayan belt: The Aegean Sea and surrounding regions, *Geophys. J. R. Astron. Soc.*, *55*, 217–254, doi:10.1111/j.1365-246X.1978.tb04759.x.

McLean, N. M., J. F. Bowring, and S. A. Bowring (2011), An algorithm for U-Pb isotope dilution data reduction and uncertainty propagation, *Geochem. Geophys. Geosyst.*, *12*, Q0AA18, doi:10.1029/2010GC003478.

Monod, O., C. Kuzucuoğlu, and A. I. Okay (2006), A Miocene palaeovalley network in the Western Taurus (Turkey), *Turk. J. Earth Sci.*, *15*, 1–23.

Morris, A., and A. H. F. Robertson (1993), Miocene remagnetisation of carbonate platform and Antalya Complex units within the Isparta Angle, SW Turkey, *Tectonophysics*, *220*, 243–266, doi:10.1016/0040-1951(93)90234-B.

Mulch, A., and C. P. Chamberlain (2007), Stable isotope paleoaltimetry in orogenic belts–the silicate record in surface and crustal geological archives, *Rev. Mineral. Geochem.*, *66*, 89–118, doi:10.2138/rmg.2007.66.4.

Nazik, A. (2004), Planktonic foraminiferal biostratigraphy of the Neogene sequence in the Adana Basin, Turkey, and its correlation with standard biozones, *Geol. Mag.*, *141*, 379–387, doi:10.1017/S0016756804009148.

Orszag-Sperber, F., A. Caruso, M.-M. Blanc-Valleron, D. Merle, and J.-M. Rouchy (2009), The onset of the Messinian salinity crisis: Insights from Cyprus sections, *Sediment. Geol.*, *217*, 52–64, doi:10.1016/j.sedgeo.2009.03.006.

Özsayın, E., and K. Dirik (2011), Regional changeover from shortening to extension: The role of oroclinal bending in the evolution of the Central Anatolian Plateau, *Geol. Carpathica*, *62*(4), 345–359, doi:10.2478/v10096-011-0026-7.

Pérez-Folgado, M., F. J. Sierro, M. A. Barcena, J. A. Flores, A. Vazquez, R. Utrilla, F. J. Hilgen, W. Krijgsman, and G. M. Filippelli (2003), Western versus eastern Mediterranean paleoceanographic response to astronomical forcing: A high-resolution microplankton study of precession-controlled sedimentary cycles during the Messinian, *Palaeogeogr. Palaeoclimatol. Palaeoecol.*, *190*, 317–334, doi:10.1016/S0031-0182(02)00612-0.

Piper, J. D. A., H. Gürsoy, O. Tatar, M. E. Beck, A. Rao, F. Koçbulut, and B. L. Mesci (2010), Distributed neotectonic deformation in the Anatolides of Turkey: A palaeomagnetic analysis, *Tectonophysics*, *488*, 31–50, doi:10.1016/j.tecto.2009.05.026.

Poisson, A., R. Wernli, E. K. Sağular, and H. Temiz (2003), New data concerning the age of the Aksu Thrust in the south of the Aksu valley, Isparta Angle (SW Turkey): Consequences for the Antalya Basin and the Eastern Mediterranean, *Geol. J.*, *38*, 311–327, doi:10.1002/gj.958.

Poisson, A., F. Orszag-Sperber, E. Kosun, M.-A. Bassetti, C. Müller, R. Wernli, and J.-M. Rouchy (2011), The Late Cenozoic evolution of the Aksu basin (Isparta Angle; SW Turkey). New insights, *Bull. Soc. Geol. Fr.*, *182*(2), 133–148, doi:10.2113/gssgfbull.182.2.133.

Quade, J., C. Garzione, and J. Eiler (2007), Paleoelevation reconstruction using pedogenic carbonates, *Rev. Mineral. Geochem.*, *66*, 53–87, doi:10.2138/rmg.2007.66.3.

Ramezani, J., M. D. Schmitz, V. I. Davydov, S. A. Bowring, W. S. Snyder, and C. J. Northrup (2007), High-precision U-Pb zircon age constraints on the Carboniferous-Permian boundary in the southern Urals stratotype, *Earth Planet. Sci. Lett.*, *256*(1–2), 244–257, doi:10.1016/j.epsl.2007.01.032.

Reilinger, R. E., S. C. McClusky, M. B. Oral, R. W. King, M. N. Toksoz, A. A. Barka, I. Kinik, O. Lenk, and I. Sanli (1997), Global Positioning System measurements of present-day crustal movements in the Arabia-Africa-Eurasia plate collision zone, *J. Geophys. Res.*, *102*(B5), 9983–9999, doi:10.1029/96JB03736.

Reilinger, R., et al. (2006), GPS constraints on continental deformation in the Africa-Arabia-Eurasia continental collision zone and implications for the dynamics of plate interactions, *J. Geophys. Res.*, *111*, B05411, doi:10.1029/2005JB004051.

Riihimaki, C., and J. Libarkin (2007), Terrestrial cosmogenic nuclides as paleoaltimetric proxies, *Rev. Mineral. Geochem.*, *66*, 269–278, doi:10.2138/rmg.2007.66.11.

Robertson, A. H. F., A. Poisson, and Ö. Akıncı (2003), Developments in research concerning Mesozoic-Tertiary Tethys and neotectonics in the Isparta Angle, SW Turkey, *Geol. J.*, *38*, 195–234, doi:10.1002/gj.953.

Roe, G. H., K. X. Whipple, and J. K. Fletcher (2008), Feedbacks among climate, erosion, and tectonics in a critical wedge orogen, *Am. J. Sci.*, *308*(7), 815–842, doi:10.2475/07.2008.01.

Rotstein, Y. (1984), Counterclockwise rotation of the Anatolian block, *Tectonophysics*, *108*, 71–91, doi:10.1016/0040-1951(84)90155-0.

Rouchy, J.-M., and A. Caruso (2006), The Messinian salinity crisis in the Mediterranean basin: A reassessment of the data and an integrated scenario, *Sediment. Geol.*, *188–189*, 35–67, doi:10.1016/j.sedgeo.2006.02.005.

Roveri, M., and V. Manzi (2006), The Messinian salinity crisis: Looking for a new paradigm?, *Palaeogeogr. Palaeoclimatol. Palaeoecol.*, *238*, 386–398, doi:10.1016/j.palaeo.2006.03.036.

Roveri, M., V. Manzi, F. Ricci Lucchi, and S. Rogledi (2003), Sedimentary and tectonic evolution of the Vena del Gesso basin (Northern Apennines, Italy): Implications for the onset of the Messinian salinity crisis, *Geol. Soc. Am. Bull.*, *115*, 387–405, doi:10.1130/0016-7606(2003)115<0387:SATEOT>2.0.CO;2.

Sahagian, D., and A. Proussevitch (2007), Paleoelevation measurement on the basis of vesicular basalts, *Rev. Mineral. Geochem.*, *66*, 195–213, doi:10.2138/rmg.2007.66.8.

Salvini, F., A. Billi, and D. U. Wise (1999), Strike-slip fault-propagation cleavage in carbonate rocks: The Mattinata fault zone, Southern Apennines, Italy, *J. Struct. Geol.*, *21*, 1731–1749, doi:10.1016/S0191-8141(99)00120-0.

Sampalmieri, G., A. Iadanza, P. Cipollari, D. Cosentino, and S. Lo Mastro (2010), Palaeoenvironments of the Mediterranean Basin at the Messinian hypersaline/hyposaline transition: Evidence from natural radioactivity and microfacies of post-evaporitic successions of the Adriatic sub-basin, *Terra Nova*, *22*, 239–250, doi:10.1111/j.1365-3121.2010.00939.x.

Santarelli, A., H. Brinkhuis, F. J. Hilgen, L. J. Lourens, G. J. M. Versteegh, and H. Visser (1998), Orbital signatures in a Late Miocene dinoflagellate record from Crete (Greece), *Mar. Micropaleontol.*, *33*, 273–297, doi:10.1016/S0377-8398(97)00042-X.

Schattner, U. (2010), What triggered the early to-mid Pleistocene tectonic transition across the entire eastern Mediterranean?, *Earth Planet. Sci. Lett.*, *289*, 539–548, doi:10.1016/j.epsl.2009.11.048.

Schildgen, T. F., K. V. Hodges, K. X. Whipple, M. S. Pringle, M. van Soest, and K. Cornell (2009), Late Cenozoic structural and tectonic development of the western margin of the central Andean Plateau in southwest Peru, *Tectonics*, *28*, TC4007, doi:10.1029/2008TC002403.

Schildgen, T. F., D. Cosentino, B. Bookhagen, S. Niedermann, C. Yıldırım, H. P. Echtler, and M. R. Strecker (2012), Multi-phased uplift of the southern margin of the Central Anatolian plateau, Turkey: A record of tectonic and upper mantle processes, *Earth Planet. Sci. Lett.*, *317–318*, 85–95, doi:10.1016/j.epsl.2011.12.003.

Schmidt, G. C. (1961), Stratigraphic nomenclature for the Adana region petroleum district VII, *Pet. Admin. Bull.*, *6*, 47–63.

Seager, R., D. S. Battisti, J. Yin, N. Gordon, N. Naik, A. C. Clement, and M. A. Cane (2002), Is the Gulf Stream responsible for Europe's mild winters?, *Q. J. R. Meteorol. Soc.*, *128*, 2563–2586, doi:10.1256/qj.01.128.

Şenel, M. (2002), Geological map of Turkey, Konya (No. 14), scale 1;500,000, 1 sheet, Maden Tetkik ve Arama Genel Müdürlüğü, Ankara.

Şengör, A. M. C. (1980), Türkiye'nin Neotektoniginin Esaslari, *Turk. Jeol. Kurumu Konf. Ser.*, *2*, 40 pp.

Şengör, A. M. C., and Y. Yılmaz (1981), Tethyan evolution of Turkey: A plate tectonic approach, *Tectonophysics*, *75*(3–4), 181–241, doi:10.1016/0040-1951(81)90275-4.

Şengör, A. M. C., S. Özeren, T. Genç, and E. Zor (2003), East Anatolian high plateau as a mantle-supported, north–south shortened domal structure, *Geophys. Res. Lett.*, *30*(24), 8045, doi:10.1029/2003GL017858.

Şengör, A. M. C., O. Tüysüz, C. İmren, M. Sakınç, H. Eyidoğan, N. Görür, X. Le Pichon, and C. Rangin (2005), The North Anatolian fault: A new look, *Annu. Rev. Earth Planet. Sci.*, *33*, 37–112, doi:10.1146/annurev.earth.32.101802.120415.

Sgarrella, F., R. Sprovieri, E. Di Stefano, A. Caruso, M. Sprovieri, and G. Bonaduce (1999), The Capo Rossello bore-hole (Agrigento, Sicily) cyclostratigraphic and paleoceanographic reconstructions from quantitative analyses of the Zanclean foraminiferal assemblages, *Riv. Ital. Paleontol. Stratigr.*, *105*(2), 303–322.

Sprovieri, R., E. Di Stefano, and M. Sprovieri (1996), High resolution chronology for late Miocene Mediterranean stratigraphic events, *Riv. Ital. Paleontol. Stratigr.*, *102*, 77–104.

Stolar, D., G. Roe, and S. Willett (2007), Controls on the patterns of topography and erosion rate in a critical orogen, *J. Geophys. Res.*, *112*, F04002, doi:10.1029/2006JF000713.

Taymaz, T., J. Jackson, and D. McKenzie (1991), Active tectonics of the north and central Aegean Sea, *Geophys. J. Int.*, *106*, 433–490, doi:10.1111/j.1365-246X.1991.tb03906.x.

Temel, A., M. N. Gündoğdu, and A. Gourgaud (1998), Petrological and geochemical characteristics of Cenozoic high-K calc-alkaline volcanisms in Konya, Central Anatolia, Turkey, *J. Volcanol. Geotherm. Res.*, *85*, 327–354, doi:10.1016/S0377-0273(98)00062-6.

Ulu, Ü. (2002), Geological map of Turkey, Adana (No. 15), scale 1;500,000, 1 sheet, Maden Tetkik ve Arama Genel Müdürlüğü, Ankara.

van Hinsbergen, D. J. J., M. J. Dekkers, and A. Koç (2010), Testing Miocene remagnetization of Bey Dağları: Timing and amount of Neogene rotations in SW Turkey, *Turkish J, Earth Sci.*, *19*, 123–156, doi:10.3906/yer-0904-1.

Whipple, K. X. (2009), The influence of climate on the tectonic evolution of mountain belts, *Nat. Geosci.*, *2*(2), 97–104, doi:10.1038/ngeo413.

Whipple, K. X., and G. E. Tucker (1999), Dynamics of the stream-power river incision model: Implications for height limits of mountain ranges, landscape response timescales, and research needs, *J. Geophys. Res.*, *104*, 17,661–17,674, doi:10.1029/1999JB900120.

Whipple, K. X., and G. E. Tucker (2002), Implications of sediment-flex dependent river incision models for landscape evolution, *J. Geophys. Res.*, *107*(B2), 2039, doi:10.1029/2000JB000044.

Whittaker, A. C., P. A. Cowie, M. Attal, G. E. Tucker, and G. P. Roberts (2007), Bedrock channel adjustment to tectonic forcing: Implications for predicting river incision rates, *Geology*, *35*(2), 103–106, doi:10.1130/G23106A.1.

Whittaker, A. C., M. Attal, and P. A. Allen (2010), Characterizing the origin, nature and fate of sediment exported from catchments perturbed by active tectonics, *Basin Res.*, *22*, 809–828, doi:10.1111/j.1365-2117.2009.00447.x.

Willett, S. D. (1999), Orogeny and orography: The effects of erosion on the structure of mountain belts, *J. Geophys. Res.*, *104*(B12), 28,957–28,981, doi:10.1029/1999JB900248.

Wobus, C. W., B. T. Crosby, and K. X. Whipple (2006), Hanging valleys in fluvial systems: Controls on occurrence and implications for landscape evolution, *J. Geophys. Res.*, *111*, F02017, doi:10.1029/2005JF000406.

Woodside, J. (1977), Tectonic elements and crust of the Eastern Mediterranean Sea, *Mar. Geophys. Res.*, *3*, 317–354, doi:10.1007/BF00285658.

Yağmurlu, F., Y. Savaşçın, and M. Ergün (1997), Relation of alkaline volcanism and active tectonism within the evolution of the Isparta Angle, SW Turkey, *J. Geol.*, *105*, 717–728, doi:10.1086/515978.

Yalçın, H. (1990), Neojen Yaşlı Kırka (Eskişehir) volkanosedimanter gölsel basenin stratigrafik ve tectonik özellikleri, *Bull. Fac. Engin. Cum. Univ, Earth Sci.*, *6–7*, 165–180.

Yalçın, N. M., and N. Görür (1984), Sedimentological evolution of the Adana Basin, in *Proceedings of the International Symposium on the Geology of the Taurus Belt, Ankara*, edited by O. Tekeli and M. C. Göncüoğlu, pp. 165–172, Maden Tetkik ve Arama Genel Müdürlüğü, Ankara.

Yıldırım, C., T. F. Schildgen, H. Echtler, D. Melnick, and M. Strecker (2011), Late Neogene and active orogenic uplift in the Central Pontides associated with the North Anatolian Fault; implications for the northern margin of the Central Anatolian Plateau, Turkey, *Tectonics*, *30*, TC5005, doi:10.1029/2010TC002756.

S. A. Bowring and R. Buchwaldt, Department of Earth, Atmospheric and Planetary Sciences, Massachusetts Institute of Technology, 77 Massachusetts Ave., Cambridge, MA 02139, USA.

A. Caruso, Dipartimento di Scienze della Terra e del Mare, Università Palermo, via Archirafi 22, I-90123 Palermo, Italy.

D. Cosentino, Dipartimento di Scienze Geologiche, Università degli Studi Roma Tre, Largo San Leonardo Murialdo 1, I-00146 Rome, Italy.

H. Echtler and C. Yıldırım, Helmholtz-Zentrum Potsdam, Deutsches GeoForschungsZentrum, Telegrafenberg, D-14473 Potsdam, Germany.

B. Rojay, Jeoloji Mühendisliği Bölümü, Orta Doğu Teknik Üniversitesi, Üniversiteler Mahallesi, Dumlupınar Bulvarı No. 1, 06800 Çankaya, Ankara, Turkey.

T. F. Schildgen and M. R. Strecker, Institute of Earth and Environmental Science, Universität Potsdam, Karl-Liebknecht-Str. 24, Haus 27, D-14476 Potsdam-Golm, Germany. (tschild@uni-potsdam.de)